



Modelling of sorption-enhanced steam reforming (SE-SR) process in fluidised bed reactors for low-carbon hydrogen production: A review

Chinonyelum Udemu, Carolina Font-Palma *

School of Engineering, University of Hull, Hull HU6 7RX, UK

ARTICLE INFO

Keywords:

Sorption-enhanced steam reforming
CO₂ capture
Hydrogen
Modelling
CFD
SE-SMR

ABSTRACT

Sorption-enhanced steam reforming (SE-SR) offers lower capital costs than conventional steam reforming with carbon capture, which arises from the compact makeup that allows reforming and CO₂ capture to occur in a single reactor. However, the technology readiness level (TRL) of SE-SR technology is currently low and large-scale deployment can be expedited by ramping up activities in reactor modelling and validation at pilot scale. This work first explores the concept of SE-SR technology, then the experimental activities and pilot tests performed for this technology, followed by the review of progress made on SE-SR modelling. It was found that the Eulerian-Eulerian two-fluid model is the most popular approach widely adopted for modelling SE-SR in fluidised bed reactors. However, the averaging method used to close equations ignores flow details at particle level and simplifies the particle system. Moreover, while hydrogen purity and yield have been predicted within an acceptable error, larger errors for CO₂ gas output relative to experimental data have been reported for this model type. Limitations and future perspectives for reactor designs and the various models and modelling approaches are also analysed, to provide guidance and advance research, modelling and scaleup of SE-SR technology.

1. Introduction

Each year, significant CO₂ emissions resulting from the direct release of the flue gas associated with the combustion of fossil fuels are recorded. There is a widespread agreement on the threats of climate change caused by CO₂ emissions and its severity if disregarded. As a result, different nations joined forces and established the historic Paris Agreement that seeks to limit increase in mean global temperature below 2 °C, ideally 1.5 °C, relative to pre-industrial levels by reducing greenhouse gas emissions [1]. Economic communities such as the European Union, the United States of America and Canada, as well as several business establishments have adopted and are highly committed to achieving net-zero emissions target [2,3]. To this end, decarbonisation strategies have been developed to accelerate progress towards achieving net-zero emission; amongst which includes the increased support and deployment of low carbon technologies such as carbon capture and low-carbon hydrogen infrastructure [4].

Hydrogen is well-recognised to possess high energy density by weight, almost thrice that of gasoline and produces water when combusted [5]. Currently, approximately 95 % of the worldwide production of hydrogen is from fossil fuels [6]. Alternative hydrogen production

routes from renewable sources are less efficient and cost-effective at large scale, therefore, fossil fuel is still expected to play a significant role towards creating a hydrogen economy [7,8]. Moreover, a review carried out by British Petroleum, BP, disclosed a surge in the volume of proved natural gas reserves from 2000 to 2020, with associating rise in demand and consumption over the recent years [9]. However, hydrogen production from fossil fuels emits 830 MtCO₂ annually [10], with steam methane reforming (SMR) identified as the leading hydrogen production technology. SMR process is regarded as the most cost-effective technology for producing high yield hydrogen at commercial scale.

Recent studies indicate that SMR with carbon capture and storage (CCS) technologies can satisfy hydrogen demand in the medium term [11]. In addition, an economic and life cycle analysis of clean hydrogen production from ten different technologies; including biomass and coal gasification, SMR, methane pyrolysis and electrolysis (wind, nuclear and solar), showed that SMR with CCS has the lowest cost of low-carbon hydrogen production [12]. Currently, there are only three commercial-scale hydrogen production facilities integrated with carbon capture and storage (CCS) technology, having a combined carbon capture capacity of ~2.1 million metric tons per year [13]. Port Arthur plant combines SMR from an existing facility and post combustion capture (PCC) technology employing vacuum swing adsorption for CO₂

* Corresponding author.

E-mail address: C.Font-Palma@hull.ac.uk (C. Font-Palma).

<https://doi.org/10.1016/j.fuel.2023.127588>

Received 18 October 2022; Received in revised form 18 January 2023; Accepted 22 January 2023

0016-2361/© 2023 The Author(s). Published by Elsevier Ltd. This is an open access article under the CC BY-NC license (<http://creativecommons.org/licenses/by-nc/4.0/>).

Nomenclature

$A_{metal\ surface}$	Catalyst's metal surface area, [m ²]
C_d	Drag coefficient
D	Diameter of reactor, [m]
$g_{o,ss}$	Radial coefficient
H	Height of reactor, [m]
K	Equilibrium constant [1/Pa]
k_1, k_2, k_3	Rate constants in R_1 , R_2 and R_3 , respectively
k_{ad}	Adsorption rate constant
k_{SMR}^0	Rate constant for SMR in NK model, [kmol/(kg s atm) ^{0.404}]
k_{WGS}^0	Rate constant for WGS in NK model, [kmol/(kg s atm)]
M	Molecular weight, [kg mol ⁻¹]
n	Parameter in the sorption rate equation
p	Partial pressure, [bar, atm]
q_{CO_2}	CO ₂ loading in adsorbent, [mol kg _{CO₂} ⁻¹]
$q_{CO_2}^*$	Adsorbent CO ₂ loading at equilibrium [mol kg _{CO₂} ⁻¹]
r_{ad}	Sorption rate, [mol/kg s]
R	Rate of reaction, [kmol/ kg _{cat} s ⁻¹]
R_1	Steam methane reforming reaction in XF model
R_2	Water-gas shift reaction in XF model
R_3	General steam methane reforming reaction in XF model
Sh	Sherwood number
T	Temperature, [K]
U	Superficial velocity [m/s]
u	Gas velocity [m/s]
Δw_{max}	Maximum CO ₂ uptake, [g CO ₂ /g absorbent]
X_{CaO}, X_{Carb}	Fractional conversion of sorbent
z	Vertical coordinate along the reactor

Abbreviations

1, 2, 3-D	One, two, three dimensional
BFB	Bubbling fluidised bed
CCS	Carbon capture and storage

CFB	Circulating fluidised bed
CFD	Computational fluid dynamics
COG	Coke oven gas
CSCM	Combined sorbent catalyst material
DEN	Denominator
GM	Grain model
ICFB	Internally circulating fluidised bed
KTGF	Kinetic theory of granular flows
LDF	Linear driving force
MSCFD	Million standard cubic feet per day
RPM	Random pore model
S/C	Steam-to-carbon ratio
SCM	Shrinking core model
SE-SMR	Sorption-enhanced steam methane reforming
SE-SR	Sorption-enhanced steam reforming
SMR	Steam methane reforming
TRL	Technology readiness level
WGS	Water-gas shift

Greek

β	Partial reaction orders for glycerol
γ	Partial reaction orders for steam
α	Transfer coefficient
ϵ	Porosity
ϵ	Voidage
ρ	Density [kg/m ³]
ζ	Bulk viscosity [Pa.s]

Subscripts

a, b, c	Co-efficient of reaction
ETD	Ethanol dehydrogenation
ACD	Acetaldehyde decomposition
i	Gas species

separation. Designed to capture 90 % CO₂, hydrogen production reaches 500 tonnes per day and is majorly used for fuel upgrading in the petroleum refinery. Quest CCS plant produces 900 tonnes of hydrogen per day in a petroleum refinery and captures CO₂ from the existing SMR using amine-based PCC, with CO₂ capture rate of 82 % [14]. Port Jerome produces hydrogen by SMR for use in the refining industry and integrated with PCC method called CRYOCAP™ where membranes and cryogenic separation are adopted for CO₂ removal. CO₂ capture rate in this facility reaches 95 %. However, current SMR plants with CCS retrofits impose a cost penalty (around \$76) per tonne CO₂ captured, and reduce the overall process efficiency (65–70 %) [11,15,16]. Moreover, construction of such conventional SMR-CCS systems to service heat and transport may not be efficient in terms of cost and high yield hydrogen production in the near future, as new and efficient technologies are continually emerging [11].

With great demand to achieve net-zero by 2050, and an increasing discovery of proven fossil fuel reserves, the transition to large-scale low-carbon hydrogen will require significant deployment of new low-carbon hydrogen plants. Opportunity still exists for the development of sustainable blue hydrogen technologies to meet the hydrogen demand necessary to reach net-zero emissions [13]. Accordingly, sorption-enhanced steam reforming (SE-SR) is an advanced blue hydrogen production technology, in which the reforming steps and CO₂ separation

steps are integrated in a single reactor. This technology offers a reduction of operational complexity and improves hydrogen yield at low cost of gas post-processing, compared with conventional hydrogen production technologies such as SMR. At present, investigations on sorption-enhanced processes are gaining popularity at both experimental and modelling level. Modelling studies are highly useful in understanding chemical processes, especially advanced technologies like SE-SR; and its successful development will help minimise experimental costs.

Sorption-enhanced processes have been reviewed in literature, as seen in Table 1, based on a broader scope. No review has been devoted to modelling studies concerning SE-SR in fluidised bed reactor at the reactor level. Therefore, this review not only focuses on highlighting the status of SE-SR models, but also its modelling approaches and reliability, while providing guidance for future modelling of SE-SR process in fluidised bed reactors. In this paper, the sorption-enhanced process by steam reforming of methane is mainly described, but also includes reforming of other raw materials. The first section will give an overview of the technology and provide a brief review of experimental and pilot studies conducted in fluidised bed reactors. The second section will focus on the models, modelling activities and approaches implemented to study SE-SR process. It is worthy to note that this review does not consider feedstocks employing solid fuels such as coal and biomass.

Table 1
Highlights of review studies concerning SE-SR process.

Authors	Review focus
Harrison [17]	General overview of research activities in sorption-enhanced process with emphasis sorbent adoption and durability.
Voldsund et al. [18]	General review of fossil-fuel based hydrogen production technologies with carbon capture such as absorption, adsorption, membrane, cryogenic separation technologies
Hanak et al. [19]	Review of progress and application of calcium-looping technologies in power generation systems including the application of sorption-enhanced process in power generation
Wang et al. [20]	Detailed review of sorbents for carbon capture including techno-economic assessment and sorbent application technologies.
Giuliano and Gallucci [21]	Review of SE-SR of methane with focus on the adoption and progress of CaO-based sorbent and Nickel-based catalyst in SE-SR of methane.
Barelli et al. [22]	Overview of methods to improve hydrogen production by SMR. Review of operating parameters for SE-SR of methane including performance of commonly used SMR and carbonation kinetic models.
Wu et al. [23]	Brief review on materials and thermodynamic studies of SE-SR with focus on developments in adsorptive reactor configuration.
Romano et al. [24]	Brief review of calcium-looping technologies modelling studies.
Soltani et al. [25]	Reviewed the impact of different process configurations of SE-SMR and the application of artificial intelligence in optimisation of SE-SMR
Sikarwar et al. [26]	Explored the various dimensions of in-situ CO ₂ capture including sorption-enhanced – gasification of solid fuels, reforming of gaseous hydrocarbons, and water–gas shift of various feedstock.

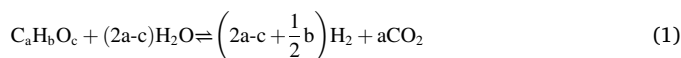
2. SE-SR technology

2.1. Process overview

The concept of sorption-enhanced reaction for hydrogen production was earlier proposed by Gluud et al. [27], in which the steam reforming and shift reactions occur in a such a manner that the produced CO₂ is removed immediately, thereby shifting the equilibrium towards more hydrogen and CO₂ production, according to Le Chatelier's principle. The steam reforming and carbonation reactions mentioned, occur in the reformer/carbonator in the presence of a catalyst and sorbent. To reduce the cost of replacing fresh sorbent after each capture cycle, the sorbent is regenerated in a calciner or regenerator. In the calciner, the sorbent is regenerated by reducing the partial pressure of CO₂ below its equilibrium either by pressure swing [28] or temperature swing [29]. Various reactor concepts have been proposed and reported for sorption-enhanced steam reforming (SE-SR), including trickle bed [30,31], fixed bed [32–40] and fluidised bed reactors.

Existing pilot scale configurations for sorption-enhanced steam reforming (SE-SR) usually involve single or two interconnected bubbling fluidised bed (BFB) reactors. In SE-SR occurring in fluidised bed reactors, the fuel and steam are usually introduced through the bottom of the reactor at a specified steam-to-carbon ratio, and a flowrate above the minimum fluidisation velocity for the binary particles (catalyst and sorbent). The reforming and water–gas shift reactions occur inside the reactor alongside the sorption reaction, with reaction temperature ranging between 550 °C and 650 °C under atmospheric conditions [35,41–44]. This combined reforming/carbonation reaction is considered to be thermally neutral, which means that the exothermic carbonation reaction provides just enough heat for the reforming reaction in the reactor [17]. Accordingly, the carbonation reaction produces CaCO₃ solids that are regenerated in the calciner operated at or above 900 °C to produce pure CO₂ stream, with heat provided directly or indirectly. The combined reforming reaction is represented in equation (1), while the carbonation/regeneration reaction is given in equation

(2).



M denotes alkali or alkaline-earth metals such as potassium, calcium, sodium, lithium and aluminium – based materials. Zeolites, metal organic frameworks, and hydrotalcites also make up the sorbents [45]. Hydrogen concentration at the outlet stream of SE-SR can reach as high as 99.31, as observed in the work of Wu et al. [46] using methanol as feedstock and hydrotalcite as sorbent; or much lesser at ~94 % [47], depending on the feedstock, sorbent and operating conditions. (Fig. 1)

Catalysts and sorbents play a crucial role in the performance of SE-SR. The development and use of solid sorbents is popular due to their lower regeneration temperature which reduces the energy penalty for CO₂ separation [48]. The choice of solid sorbent for CO₂ capture in SE-SR has been reported to be dependent on a number of other factors including: kinetics of adsorption and desorption, adsorption capacity, cost, performance and stability after multiple carbonation – regeneration cycles [22]. On the other hand, the criteria for catalyst selection include high thermal and mechanical stability, high activity at high temperatures, increased life time and efficient heat transfer [49]. Nickel catalyst is the most widely adopted catalyst for steam reforming compared to other noble metals such as platinum, iridium and rhodium. However, due to the tendency of these catalysts and sorbents to sinter at high steam-to-carbon ratio, a great deal of development is being made towards the improvement of these materials. A more compact material made by the combination of sorbent and catalyst is found to be feasible for application in SE-SR. These materials are referred to as bifunctional catalysts or combined sorbent catalyst materials [21,50], and have been widely reported in literature for use in hydrogen production via SE-SR. They benefit from the minimisation of particle sintering, low solid holdup in the reactor, little or no particle separation, better integration of exothermic and endothermic reactions and improved inter-particle flow [21].

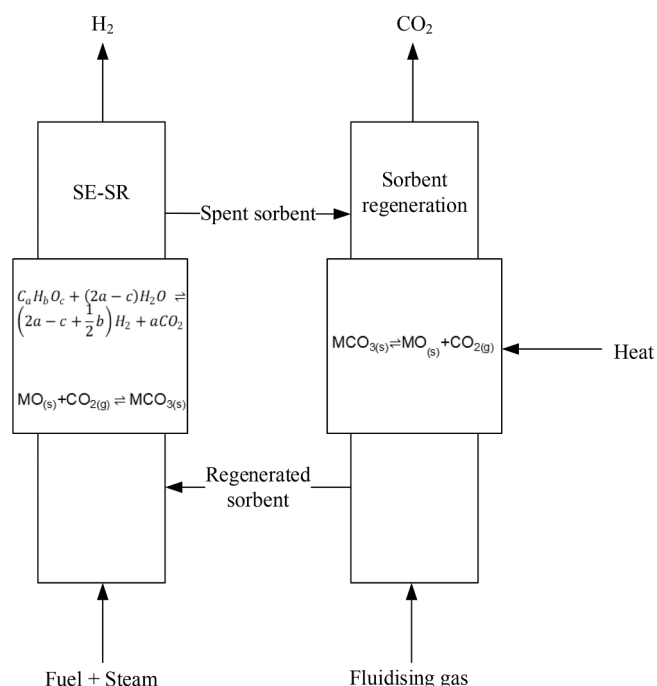


Fig. 1. Schematic diagram of the sorption-enhanced steam reforming process.

2.2. Thermodynamics and effect of operating conditions

A thermodynamic analysis of SE-SR of methane using a calcium-based sorbent shows that an equilibrium hydrogen content of >95 % can be attained at steam-to-carbon ratio of 4, pressure of 15 atm, and temperatures below 750 °C [51]. A maximum hydrogen content of 96 % can be obtained at 650 °C, in addition to a highly efficient carbonation reaction. Although hydrogen purity increases with temperature due to high methane conversion, the CO₂ separation efficiency is highly reduced at temperatures above 850 °C and desorption occurs. It has also been reported that even higher pressures up to 30 bar for SE-SR reduces the hydrogen purity and methane conversion but improves the carbonation reaction [52]. (Fig. 2)

Factors such as temperature, pressure, steam-to-carbon ratio are

known to affect hydrogen production by SE-SR processes in similar ways as described by thermodynamics. Temperature is a fundamental quantity that affects hydrogen purity and yield, as well as efficiency. At higher temperatures, fuel conversion is favoured due to endothermic steam reforming reaction, whereas CO₂ removal is inhibited due to the exothermic carbonation reaction [35]. Thus, CO₂ and hydrogen are increased and reduced respectively in the prebreakthrough periods. Therefore, an optimum temperature at which hydrogen purity is improved whilst reducing outlet CO₂ composition, must be determined. Barelli et al. [22] divided the typical response from a sorption-enhanced reactor into start-up region – period of catalyst reduction and activation; prebreakthrough period – equilibrium for SE-SR is reached and maximum concentration can be obtained for all components; breakthrough period – all sorbent has been converted and H₂ begins to reduce;

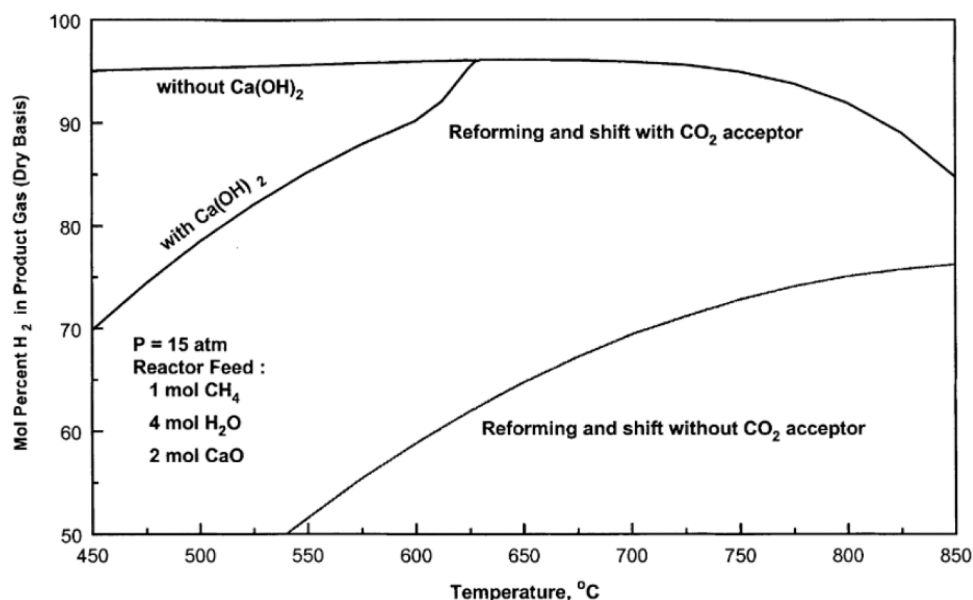


Fig. 2. Hydrogen yield at equilibrium with and without CO₂ sorbent (reused from Balasubramanian et al. [51], with permission from Elsevier).

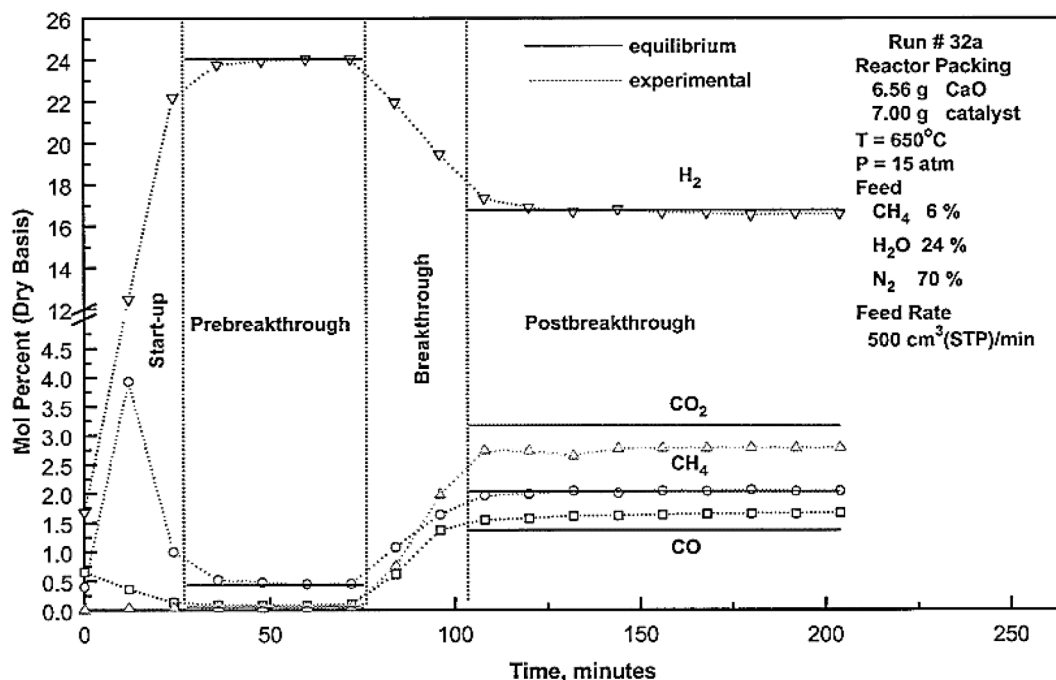


Fig. 3. Reactor response profile for SE-SR of methane (reused from Balasubramanian et al. [51], with permission from Elsevier).

and post-breakthrough period – corresponding to the absence of adsorption and dominance of steam reforming. (Fig. 3)

High steam-to-carbon (S/C) ratio has also been known to improve hydrogen concentration in the product stream [35]. Experimental trends for SE-SR show that the average S/C ratio used in experiments is 3 for methane but up to 6 for ethanol and glycerol. This implies that steam-to-fuel ratio is entirely subject to the type of feedstock adopted and will increase with the carbon content of the feed. However, due to increased plant cost imposed by higher steam-to-carbon ratios, an optimum is advised. Furthermore, the trend in published works shows that almost 80 % of the experiments are carried out in fixed bed reactors, possibly due to ease of operation at lab scale while a few are performed in bubbling fluidised bed reactors. However, it is important to perform more SE-SR experiments in fluidised bed reactors, as these are more appropriate for large scale applications. This will also improve modelling and validation studies and enable understanding the challenges associated with continuous operation mode for the process, even at large scale.

2.3. Review of experimental and pilot tests in fluidised bed reactors

Experiments are important in model validation, to ensure the reliability and accuracy of the model in process analysis. Few experiments have been conducted for SE-SR in fluidised bed reactors and main achievements are described here.

2.3.1. Lab-scale fluidised bed reactors

An experiment conducted by Johnsen et al. [53] is popularly employed in model validation of SE-SR of methane in BFB reactors. In their work, a lab scale BFB reactor of height (without the expansion section) – 0.66 m and inner diameter of 0.1 m was used to study the performance of SE-SR of methane within the bubbling regime. Sorbent regeneration was also carried out sequentially in the same reactor at 850 °C. Under a catalyst/dolomite mass ratio of 2.5, S/C ratio – 3, reforming temperature and pressure of 600 °C and 1 atm respectively;

hydrogen composition reached 98–99 vol% dry basis for up to 180 min, after 4 carbonation–calcination cycles. The duration reduces because of reduced sorption capacity of the dolomite sorbent caused by the increasing number of cycles. Similar results showing reduced sorption capacity with increasing carbonation–calcination cycles have also been reported by Hildenbrand et al. [54].

In the experiment by Hildenbrand et al. [54], the performance of natural dolomite sorbent during SE-SR of methane was examined in a fluidised bed reactor of inner diameter 25 mm. They reported the existence of an induction period, during which calcium hydroxide ($\text{Ca}(\text{OH})_2$) is produced by the reaction of CaO with water vapour. This induction period is found to be dependent on temperature and steam-to-carbon ratio, with elevated temperatures and steam-to-carbon ratios reducing the induction time. Low hydrogen yield was observed during this period, due to the subsequent reduction in steam, following the formation of $\text{Ca}(\text{OH})_2$.

Martínez et al. [55] compared the performance of a synthetic CaO -based sorbent and reforming catalyst compared with a combined sorbent catalyst material (CSCM) under relevant operating conditions. An SE-SR experiment was conducted in a batch fluidised bed reactor of length – 853 mm, internal diameter – 53.1 mm and distributor plate located 586 mm from top reactor. The same reactor was adopted for the calcination of the sorbent in a steam-rich environment and in the presence of small hydrogen. The CO_2 sorption capacity of the CSCM was the same as that of the separate sorbent particles and H_2 purity reached 96 %. The presence of at least 4 vol% H_2 within the calciner was recommended to prevent the deactivation of the catalyst due to oxidation. (Fig. 4)

More recently, García et al. [56] experimentally investigated the performance of SE-SR of biogas in an updraft fluidised bed reactor and compared the results with the conventional biogas reforming. The reactor, which has an inner diameter of 27 mm, was loaded with dolomite sorbent and nickel-based hydrotalcite catalyst materials at a sorbent-to-catalyst ratio of ≥ 5 g/g for the experimental runs. Hydrogen purity of 98.4 vol% was obtained at 550–600 °C before it reduced with

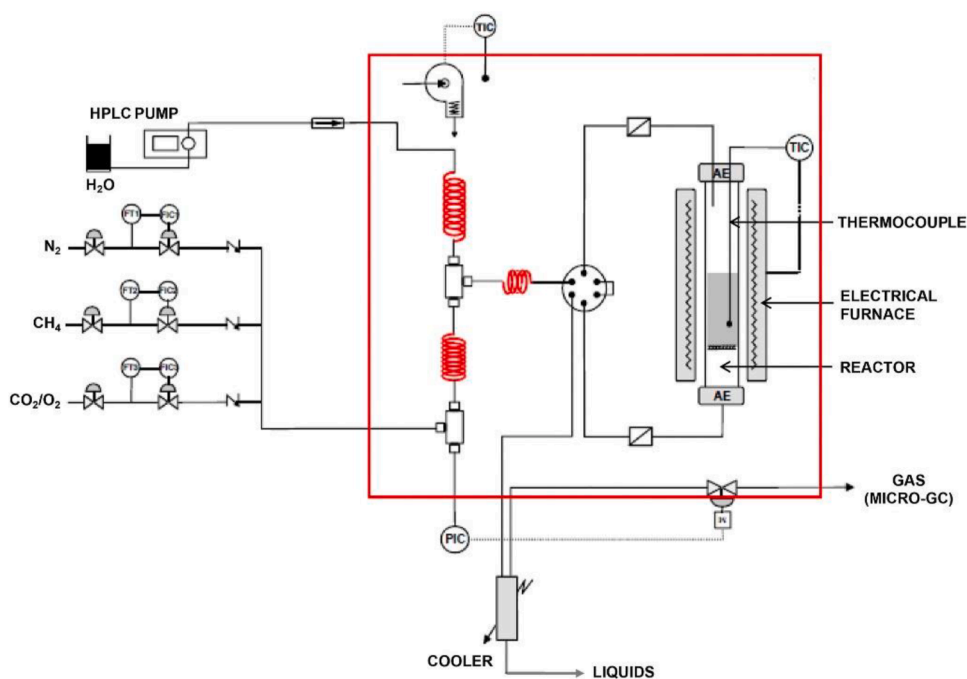


Fig. 4. Laboratory set-up for SE-SR of biogas (reused from García et al. [56], with permission from Elsevier).

an increase in temperature, whereas the hydrogen yield obtained at 650 °C was 93.2 % for methane and 92.7 % for biogas.

SE-SR is still transitioning to TRL 6; therefore, few pilot test facilities are in existence. For example, a 1.5MWh pilot plant is currently being developed at Cranfield University, UK to produce blue hydrogen, with the major aim of demonstrating SE-SR under high pressure conditions (up to 30 bar) while improving the process economics [57]. A brief review of the pilot operations performed in currently existing pilot plants will be provided below, with the goal of identifying key operating parameters and results, useful for modelling studies and validation.

2.3.2. Pilot test facilities for SE-SR

2.3.2.1. Institute for energy technology, IFE Hynor. IFE, Hynor operates the Hydrogen Technology Centre consisting of a high temperature solid oxide fuel cell (SOFC) technology integrated with a hydrogen reformer pilot plant. The reformer system is a dual bubbling fluidised bed prototype that produces hydrogen by sorption-enhanced steam reforming of methane [58]. The 30kW_{H2} pilot plant has a reformer/carbonator which is a bubbling fluidised bed with freeboard height, freeboard inner diameter and bed diameter of 1.20 m, 0.348 m and 0.2545 m respectively, interconnected to a bubbling bed calciner and a riser unit for transport. To improve heat integration, a high temperature heat exchanger is submerged in the calciner which is dimensioned to account for the heating surface for the decarbonation reaction. A riser with height, 4.5 m and inner diameter, 0.067 m transports the solids from the reformer to the calciner using the reformat gas (contains minor quantities of CO₂, CO, unconverted CH₄ and N₂). The operating conditions for the reformer/carbonator and the calciner are 600 °C and 850 °C respectively, at near atmospheric pressure and using dolomite sorbent and nickel catalyst. (Fig. 5)

A first batch test of the plant was run at reformer condition – 600 °C, fluidisation velocity – 0.29 m/s, steam to carbon ratio – 4 and sorbent to catalyst mass ratio of 2.8, using upgraded biogas as the feedstock. A stable hydrogen concentration of 95 % vol and high carbon capture rate was obtained and temperature distribution across the reactor bed was

reported to be uniform, validating the feasibility of operating the process under such conditions. The regeneration batch test, first powered up by electricity before stabilizing with the burner, exhibited a linear and even temperature increase across the bed. However, tests are ongoing to operate these reactors as a loop, coupling the solid circulation in continuous mode.

2.3.2.2. Gas Technology Institute (GTI) Hydrogen Technology. GTI has piloted an SE-SR process termed the compact hydrogen generator (CHG), with hydrogen production capacity of 20 MSCFD (~48 kg/day) and located at Energy and Environment Research Centre (EERC) in Grand Forks, North Dakota [60]. The pilot plant consists of reformer/carbonator fluidised bed reactor loaded with ~11 kg of nickel-based catalyst and CaO sorbent that is elutriated through the bed, a stand-pipe which temporary stores the CaCO₃ to be regenerated and an indirectly fired rotary kiln calciner. The reformer is operated at 700 °C, steam to carbon ratio of 3 and 1–3 atm pressure, whereas the calciner temperature is maintained at 850–900 °C. Sorbents of small particle sizes (<10 μm) is adopted for rapid release of CO₂ within a short residence time in the calciner, to mitigate sorbent decay and sintering caused by high temperature exposure. The standpipe is also controlled at hydraulic head of about 0.14–0.2 atm to prevent pressure differences between the reactor system as well as separate hydrogen product gases and burner gases, coupled with a rotary valve at the bottom to direct solids into the calciner. (Fig. 6)

Four tests were carried out in the plant in 2016, with the first test riddled with challenges arising from design and installation: rotor damage and inability to seal burner hat. However, subsequent tests proved successful culminating in ~80–90 % hydrogen purity, 90 % CO₂ capture rate and minimisation of catalyst degradation. The fourth test to increase the feed rate to design rate was successful but hydrogen purity was reduced due to low sorbent activity. Finally, the total pilot plant operational time reportedly reached 88+ hours of SER operation and more than 200 h of solids handling operation, achieving >92 % hydrogen purity and 90 % carbon capture rate [62].

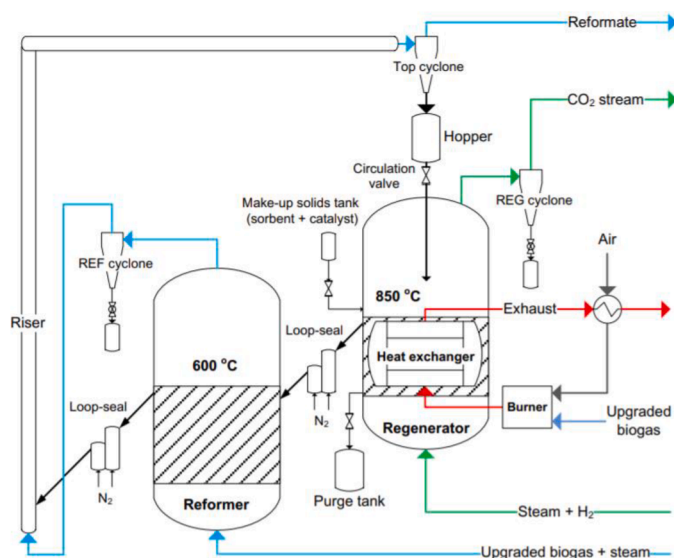


Fig. 5. Design of the dual bubbling fluidised bed SER plant at IFE (reused from Meyer et al. [59], with permission from Elsevier).

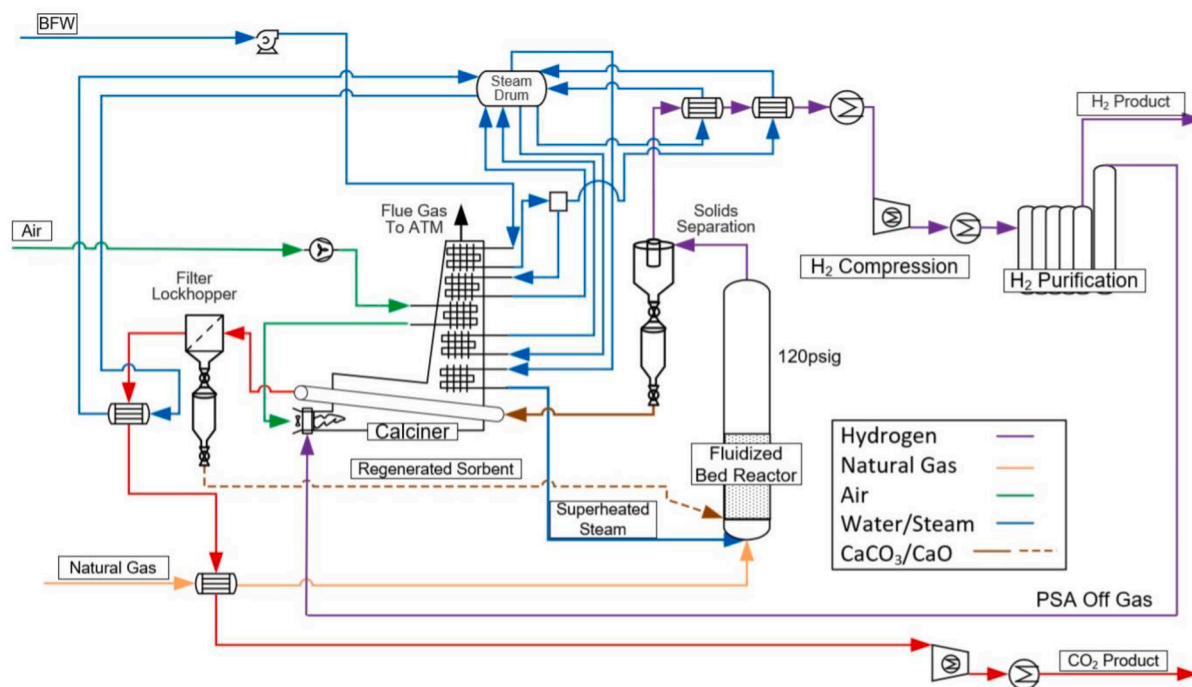


Fig. 6. Process flow diagram of GTI's compact hydrogen generator pilot plant (reused with permission from Mays et al. [61]).

3. Models for SE-SR process

Modelling studies are incredibly useful in developing an understanding of chemical processes, especially modern technologies like SE-SR. Rigorous modelling work will accelerate the deployment of SE-SMR technology, as these studies will expose complications and bottlenecks, as well as provide solutions, associated with the process at large scale. This section aims to provide insights on the status of SE-SR models and modelling approaches, highlight model reliability and drawbacks, and provide guidance for future modelling works, in order to advance SE-SR technology. The increasing interest in SE-SR as a technology for low carbon hydrogen production is the main driver for this section.

The overall mathematical model can vary depending on the scale (lab to large), spatial dimension (1D, 2D and 3D) and state (steady and dynamic). Modelling of reactive flows like SE-SR in fluidised bed reactor incorporates bed fluid dynamics (hydrodynamics) and the chemical reaction kinetics models. The hydrodynamic models are categorised into the conventional fluidisation models and CFD models, while the kinetic models depend on the type of sorbent and feedstock employed, which is different for each feed and catalyst type.

3.1. Kinetic models

In SE-SR, kinetic models are developed for the reforming, carbonation/sorption and decarbonation reactions as described here.

3.1.1. Steam reforming reactions

SE-SR of methane using nickel-based catalyst and calcium oxide (CaO) as sorbent are predominantly used, due to their natural abundance and well-established kinetics. Several kinetic models have been developed to describe steam methane reforming (SMR) kinetics using elaborate reaction mechanisms, different kinetic approaches and over various catalysts. One of the earlier kinetic studies performed for steam methane reforming over nickel reported that the reaction of steam with methane is first order relative to methane, with methane decomposition being the rate-determining step [63]. This model neglects diffusion limitation of the gases in the derivation of the rate equation and could be difficult in its prediction of product distribution. A subsequent kinetic

model proposed that the desorption of carbon monoxide and carbon dioxide is the rate determining step [64]. The complexities and conflicting description of SMR kinetic models resulted in the development of more exhaustive models by other researchers.

In SE-SR of methane over nickel catalyst, kinetic models by Numaguchi and Kikuchi (NK) [65], and Xu and Froment (XF) [66] are commonly applied. The NK model considered the Langmuir-Hinshelwood and power law type approach to develop a hybrid rate equation for SMR, while assuming surface reaction as the rate-controlling step. The model was studied for reaction temperatures and pressure up to 1160 K and 25 bar, respectively. Conversely, Xu and Froment [66] presented a number of possible chemical reactions and generated 21 set of rate equations from developed reaction schemes, in their kinetic study of SMR over Ni/MgAl₂O₄ catalyst. They used the Langmuir-Hinshelwood approach to describe and formulate the reaction step and rate equation. Their mechanism indicated that CO and CO₂ are formed in parallel out of the methane adsorbed onto the catalyst, with the predicted rate reported to be dependent on the partial pressure of hydrogen. Although this model has been criticised for being complex and misrepresenting the mechanism of methane dissociation [67], it is widely adopted to model processes involving SMR on Ni-based catalysts. This is probably because all the possible reaction mechanisms involved in SMR as well as the diffusion limitations, were considered in the determination of the intrinsic rate equation. A summary of the reforming reaction applied to SE-SR is presented in Table 2.

Different kinetic models are developed for different catalyst systems because the variation of catalyst composition affects the parameters obtained and mechanisms in the kinetic model, thereby creating difficulty in the derivation of a general rate equation applicable for different catalysts [70]. Other kinetic models with associated rate expressions for SMR on various catalyst systems have been proposed using different kinetic modelling approaches. Power law approach was used to develop kinetic models for SMR on Rh-Ni/MgAl₂O₄ catalyst and Ni-YSZ (yttria-stabilized zirconia) cermet by Katheria et al. [71] and Sugihara et al. [72], respectively. Other kinetic models employing Langmuir-Hinshelwood approach have been developed for Ni/a-Al₂O [73], Nickel/Calcium Aluminate [70] and LaNiO₃ perovskite-type oxide [74] catalyst systems.

Table 2
Rate equations for steam reforming reactions applied to SE-SR.

Ref.	Reactions	Rate equations (kmol.kg _{cat} ⁻¹ .s ⁻¹)	Equation
Methane [66]	$R_1 : \text{CH}_4 + \text{H}_2\text{O} \rightleftharpoons \text{CO} + 3\text{H}_2$ $R_2 : \text{CO} + \text{H}_2\text{O} \rightleftharpoons \text{CO}_2 + \text{H}_2$ $R_3 : \text{CH}_4 + 2\text{H}_2\text{O} \rightleftharpoons \text{CO}_2 + 4\text{H}_2$	$R_1 = \frac{k_1}{P_{\text{H}_2}^{2.5}} \left[\frac{P_{\text{CH}_4} P_{\text{H}_2\text{O}} - \frac{P_{\text{H}_2}^3 P_{\text{CO}}}{K_1}}{\text{DEN}^2} \right]$ $R_2 = \frac{k_2}{P_{\text{H}_2}} \left[\frac{P_{\text{CO}} P_{\text{H}_2} - \frac{P_{\text{H}_2} P_{\text{CO}_2}}{K_2}}{\text{DEN}^2} \right]$ $R_3 = \frac{k_3}{P_{\text{H}_2}^{3.5}} \left[\frac{P_{\text{CH}_4} P_{\text{H}_2\text{O}}^2 - \frac{P_{\text{H}_2}^4 P_{\text{CO}_2}}{K_3}}{\text{DEN}^2} \right]$ $\text{DEN} = 1 + K_{\text{CH}_4} P_{\text{CH}_4} + K_{\text{CO}} P_{\text{CO}} + K_{\text{H}_2} + \frac{K_{\text{H}_2\text{O}} P_{\text{H}_2\text{O}}}{K_{\text{H}_2}}$	3456
Methane [65]	SMR: $\text{CH}_4 + \text{H}_2\text{O} \rightleftharpoons \text{CO} + 3\text{H}_2$ WGS: $\text{CO} + \text{H}_2\text{O} \rightleftharpoons \text{CO}_2 + \text{H}_2$	$r_{\text{SMR}} = \frac{k_{\text{SMR}}^0 \cdot \exp\left(-\frac{E_{\text{SMR}}}{RT}\right) (P_{\text{CH}_4} P_{\text{H}_2\text{O}} - \frac{P_{\text{CO}} P_{\text{H}_2}^3}{K_{\text{SMR}}})}{P_{\text{H}_2\text{O}}^{1.596}}$ $r_{\text{WGS}} = \frac{k_{\text{WGS}}^0 \cdot \exp\left(-\frac{E_{\text{WGS}}}{RT}\right) (P_{\text{CO}} P_{\text{H}_2\text{O}} - \frac{P_{\text{CO}_2} P_{\text{H}_2}}{K_{\text{WGS}}})}{P_{\text{H}_2\text{O}}}$	78
Ethanol [68]	$r_1 : \text{C}_2\text{H}_6\text{O} \rightleftharpoons \text{C}_2\text{H}_4\text{O} + \text{H}_2$ $r_2 : \text{C}_2\text{H}_4\text{O} \rightleftharpoons \text{CO} + \text{CH}_4$ $r_3 : \text{CH}_4 + \text{H}_2\text{O} \rightleftharpoons \text{CO} + 3\text{H}_2$ $r_4 : \text{CO} + \text{H}_2\text{O} \rightleftharpoons \text{CO}_2 + \text{H}_2$	$r_1 = \frac{k_{\text{ETD}} P_{\text{C}_2\text{H}_6\text{O}}}{\text{DEN}} \left(1 - \frac{1}{K_{\text{ETD}}} \cdot \frac{P_{\text{C}_2\text{H}_4\text{O}} P_{\text{H}_2}}{P_{\text{C}_2\text{H}_6\text{O}}} \right)$ $r_2 = \frac{k_{\text{ACD}} P_{\text{C}_2\text{H}_4\text{O}}}{\text{DEN}} \left(1 - \frac{1}{K_{\text{ACD}}} \cdot \frac{P_{\text{CO}} P_{\text{CH}_4}}{P_{\text{C}_2\text{H}_4\text{O}}} \right)$ $r_3 = \frac{k_{\text{SMR}} P_{\text{H}_2\text{O}} P_{\text{CH}_4}}{\text{DEN}^2} \left(1 - \frac{1}{K_{\text{SMR}}} \cdot \frac{P_{\text{CO}} P_{\text{H}_2}^3}{P_{\text{H}_2\text{O}} P_{\text{CH}_4}} \right)$ $r_4 = \frac{k_{\text{WGS}} P_{\text{H}_2\text{O}} P_{\text{CO}}}{\text{DEN}^2} \left(1 - \frac{1}{K_{\text{WGS}}} \cdot \frac{P_{\text{CO}_2} P_{\text{H}_2}}{P_{\text{H}_2\text{O}} P_{\text{CO}}} \right)$ $\text{DEN} = 1 + K_{\text{CH}_4} P_{\text{CH}_4} + K_{\text{EtOH}} P_{\text{EtOH}} + K_{\text{H}_2\text{O}} P_{\text{H}_2\text{O}}$	910111213
Glycerol [69]	$\text{C}_3\text{H}_8\text{O}_3(\text{g}) + 3\text{H}_2\text{O}(\text{g}) \rightleftharpoons 3\text{CO}_2(\text{g}) + 7\text{H}_2(\text{g}) + 345\text{kJ/mol}$	$R_1 = (\nu_i) A e^{-E_a/RT} P_{\text{C}_3\text{H}_8\text{O}_3}^\beta P_{\text{H}_2\text{O}}^\gamma A_{\text{metalsurface}}$	14

($\nu_i = -1$ or $+1$, if species i is being consumed or produced, respectively).

Furthermore, the rate expression for ethanol steam reforming (ESR), catalysed by nickel catalyst, is based on Langmuir-Hinshelwood-Hougen-Watson kinetic model developed by Wu et al. [68], which considers four reaction pathways – ethanol dehydrogenation, acetaldehyde decomposition, steam reforming and water gas shift. Other rate expressions for ESR often used combine the power rate law-based ethanol decomposition developed by Mas et al. [75] with the SMR rate expressions of Xu and Froment [66]. In the case of glycerol steam reforming, the reaction rate is derived using the power law approach, with the main reaction being glycerol decomposition and SMR.

3.1.2. Carbonation reactions

Carbonation involves the reaction of CO₂ with alkali or alkaline-earth metal oxides-based sorbents or any other material such as layered double hydroxides, hydrotalcite, zeolites capable of adsorbing CO₂ [20,76]. Rate expressions for these reactions can be developed based on a typical gas–solid heterogenous kinetic models [77]. The generic model for carbonation is expressed as [77];

$$\frac{dx}{dt} = kf(P_a)F(x) \tag{15}$$

Where $f(P_a)$ represents the driving force in terms of CO₂ partial pressure and is based on the order of reaction. The definition of $F(x)$ is a function of conversion and is based on any of the particle kinetic models such as shrinking core, grain and pore models. According to the shrinking core model, the reaction progresses from the surface to the middle of the particle, leaving behind a thin product layer. It separately describes the surface reaction and product layer diffusion, leading to separate equations developed for both regions [78]. This model has been used to describe the kinetics of dolomite as presented in Table 3 [79]. A parameter, n was introduced to account for the nonlinear driving force.

Alternatively, the grain model considers how grain size distribution changes with the reaction [78]. Stando and Foscolo [80] used the

grain model to describe the behaviour of dolomite carbonation, while accounting for the dramatic decrease in the rate of carbonation that the shrinking core model was unable to explain. Similarly, Sun et al. [81] established an intrinsic rate expression for the carbonation of limestone and dolomite using a grain model. The rate constants were determined for each driving force (based on CO₂ partial pressures) less than and greater than 10 kPa, respectively. Grain models have also been developed by a few authors for bifunctional pellets, assuming a constant volume and spherical pellets [40,82]. Aloisi et al. [82] successfully validated with experimental data, a pellet model developed for a new multifunctional catalyst for SE-SR of methane. The model was proven to describe the catalytic and sorption considering sorbent decay, with sensitivity analysis of sorbent grain size performed to account for sintering.

Pore models assume that the reaction proceeds by initially filling small pores before the diffusion process occurs [78]. Its variation, a three-dimensional random pore model (RPM), imagines the reacting solid surface to be the result of randomly overlaid cylindrical surfaces with specified pore size distribution and has been modified for applications in SE-SR. The RPM for fluid–solid reactions originally proposed by Bhatia and Perlmutter [83] has taken on a variety of forms to account for sorbent multi-cycling in SE-SR process [84].

In addition, apparent kinetic models that describes reaction kinetics in a simple and transparent way without the use of morphological measurements, can also be employed to describe carbonation in SE-SR [85]. Other sorption diffusion kinetics models such as the linear driving force (LDF) model have also been proposed [86]. LDF model features a driving force based on the linear difference between the equilibrium and actual adsorption amounts, as well as a proportionality constant, taking into consideration the adsorbent’s intraparticle diffusional resistance. It is worthy to note that the conversion for CaO-based sorbent is usually assumed to be below 28 % due to reduced sorbent usage and degradation during CaO multi-cycling.

Table 3
Rate equations adopted for carbonation in SE-SR.

Sorbent [Ref.]	Kinetic models	Rate equations	Equation
Dolomite [79]	SCM	$r_c = \frac{\frac{3}{R_p}(1 - X_{CaO})^{\frac{2}{3}} \frac{1}{RT}(P_{CO_2} - P_{CO_2,eq})^n}{\frac{1}{k_4} + \frac{R_p \left[(1 - X_{CaO})^{\frac{2}{3}} - (1 - X_{CaO})^{\frac{1}{3}} \right]}{D_e} + \frac{2}{k_g} (1 - X_{CaO})^{\frac{2}{3}}}}$	16
Dolomite [80], Bifunctional catalyst [82]	GM	$r_c = \frac{\sigma_{0,CaO} k_s (1 - X_{Carb})^{2/3} (C_{CO_2} - C_{CO_2,eq})}{1 + \frac{k_s N_{Ca}}{2D_{PL}} \delta_{CaO} \sqrt{1 - X_{Carb}} \left(1 - \sqrt[3]{\frac{1 - X_{Carb}}{1 - X_{Carb} + X_{Carb} Z}} \right)}$	17
Dolomite [81]	GM	$r_c = \frac{dX}{dt} = k_C (P_{CO_2} - P_{CO_2,eq})^n S(1 - X_{CaO})$	18
		$k_C = \begin{cases} 1.04 \times 10^{-4} \exp\left(\frac{-E}{RT}\right) & \text{at } P_{CO_2} - P_{CO_2,eq} \leq 10 \text{ kPa ; } n = 1 \\ 1.04 \times 10^{-3} \exp\left(\frac{-E}{RT}\right) & \text{at } P_{CO_2} - P_{CO_2,eq} > 10 \text{ kPa ; } n = 0 \end{cases}$	19
Limestone [81]	GM	$r_c = \frac{dX}{dt} = k_C (P_{CO_2} - P_{CO_2,eq})^n S(1 - X_{CaO})$	20
		$k_C = \begin{cases} 1.67 \times 10^{-3} \exp\left(\frac{-E}{RT}\right) & \text{at } P_{CO_2} - P_{CO_2,eq} > 10 \text{ kPa ; } n = 0 \\ 1.67 \times 10^{-4} \exp\left(\frac{-E}{RT}\right) & \text{at } P_{CO_2} - P_{CO_2,eq} \leq 10 \text{ kPa ; } n = 1 \end{cases}$	21
Limestone [87]	Apparent	$\frac{dX}{dt} = k_C (C_{CO_2} - C_{CO_2,eq})^{0.37} \left(1 - \frac{X_{Carb}}{X_U} \right)^{2.61}$	22
Limestone, dolomite [84]	RPM	$\frac{dX}{dt} = k_C (C_{CO_2} - C_{CO_2,eq})^{(P/P_0)^{0.083}} \left(1 - \frac{X_N}{X_{U,N}} \right)^{2/3}$	23
Hydrotalcite [86,88]	LDF	$\frac{\delta q_{CO_2}}{\delta t} = K_{LDF} (q_{CO_2}^* - q_{CO_2})$	24
LiO-based [77]	Apparent	$\frac{dX}{dt} = K (P_{CO_2} - P_{CO_2,eq})^n \left(1 - \frac{q}{q_{max}} \right)$	25
Lithium zirconate [89]	Apparent	$r_{ad} = \frac{\Delta W_{max}}{M_{CO_2}} k_{ad} C_{CO_2}^n \left(1 - \frac{\Delta W}{\Delta W_{max}} \right)$	26

3.1.3. Decarbonation/calcination reactions

SE-SR is ideally operated in a cyclic manner, where regenerated sorbent is recycled back to the carbonator, thus affecting the texture of the sorbent and in turn the kinetics of the carbonation and calcination. Under this condition, Okunev et al. [90] analysed decarbonation rates data obtained from experiments for a CaO-based sorbent. A rate expression for decarbonation of CaO was formulated in terms of CO₂ pressure, sorbent texture, Sherwood number and temperature. For SE-SR process employing CaO-based sorbent, the decarbonation model by Okunev et al. [90] is popularly employed and is presented in equation (27).

$$r_{decay} = \frac{1}{M_{CO_2}} \frac{2.46 \times 10^4 S_p \exp\left[\frac{-20474}{T}\right]}{\left[16 \frac{d_p^2 S_{sp} \rho_p}{\epsilon^2 Sh}\right]^{2/3} + \exp\left[7.8 \left(\frac{PCO_2}{PCO_{2,eq}}\right)\right]} \left(1 - \frac{PCO_2}{PCO_{2,eq}}\right) \quad (27)$$

3.2. Hydrodynamic models

Hydrodynamic models delineate the behaviours and interactions between the gas–solid and solid–solid flows for the various fluidisation regimes characterised by variations in gas velocity. The original hydrodynamic model developed by Toomey and Johnstone [91] and later improved by Kunii et al. [92] describes bed dynamics using bubble action. Though, hydrodynamic models for fluidised bed reactors have been expanded to include the rising CFD models.

3.2.1. Conventional fluidisation models

In bubbling fluidised beds, the conventional fluidisation models are the two-phase model – postulated by Toomey and Johnstone which was later improved by Davidson and Harrison [93]; and the three-phase model – developed by Kunii-Levenspiel [92]. These models use bubble motion to describe the behaviour of fluidised beds, thus limiting its application to bubbling fluidised bed reactor, and are usually empirical or non-predictive [94]. Several modifications to the originally proposed two and three phase models have gone on to be developed. One of such models is the Orcutt model which has been applied to SE-SR of methane [79].

In this modelling approach, a differential slice (see Fig. 7) is taken across any height of the reactor (reformer/carbonator) for the bubble and emulsion phases. Mass and energy balances are then written for each phase (gas and solid) in the bubble and emulsion phases, with an interphase mass transfer coefficient used to represent the mass exchange

Table 4
Relevant constitutive correlations in conventional fluidisation model.

Parameters	Equations	Unit	Equation	Ref.
Minimum fluidisation velocity	$u_{mf} = Re_{p,mf} \frac{\mu_g}{d_p \rho_g}$ $Re_{p,mf} = \sqrt{33.7^2 + 0.0408Ar} - 33.7$ $Ar = \frac{1.75}{(\epsilon_{mf}^3 \phi)} Re_{p,mf}^2 + \frac{150(1 - \epsilon_{mf})}{(\epsilon_{mf}^2 \phi^2)} Re_{p,mf}$	m/s	28	[95]
Bubble voidage fraction	$\epsilon_b = \frac{u - u_{mf}}{u_b}$	-	29	
Bubble rise velocity	$U_b = 0.711 \sqrt{g d_b}$	m/s	30	[93]
Bubble size	$d_b = d_{bm} - (d_{bm} - d_{b0}) \exp\left(\frac{-0.3z}{d_t}\right)$	m	31	[96]
Interphase mass transfer coefficient	$k_{be} = 0.75 U_{mf} + \frac{0.975 g^{0.25} D^{0.5}}{d_b^{0.25}}$	1/s	32	[92]

between both phases. The resulting equations are partial differential equations which must be solved numerically along with their constitutive correlations. Whilst some of the hydrodynamic parameters including minimum fluidisation velocity, bubble rise velocity, bubble size and bed voidage are presented in Table 4, more details on these variables are available in literature [92–94].

Other fluidisation models have also been postulated to describe flow structures and transition from the various existing fluidisation regimes. For circulating fluidised beds which mostly operate in the fast fluidisation regime, these models have been classified into three types: (1) models capable of predicting the axial variation in density of solids suspension only, (2) models that assume two or more phases to predict radial variations, and (3) models that describe gas–solid flow using the principles of fluid dynamics [97]. While the Type 2 models have been loosely adopted to model SE-SR in a CFB [98], Type 3 models (including CFDs) are commonly used in the modelling SE-SR process in fluidised bed systems.

3.2.2. CFD models

CFD approach employs the conservation law of fluid dynamics to predict gas–solid flow behaviour in fluidised beds. This approach has been proven to depict bubble formation, growth and decay for a continuous flow [99] and can be used for a wide range of fluidisation regimes. Modelling of the conservation equations (mass, momentum and energy) for the solid and gaseous phases requires that the phases be described using any of the following approaches depending on the level of detail sought; Eulerian-Lagrangian (E-L) or Eulerian-Eulerian (E-E) [100]. E-L approach treats gas phase as a continuum whereas solids are treated as discrete phase and particle motion is tracked. Two classes of Eulerian-Lagrangian approach exist: discrete element method (DEM) and dense discrete phase model (DDPM) [101], with the later recently used to model the sorption-enhanced process. However, the Eulerian-Eulerian (multi-fluid or two-fluid model) approach is widely applied in the literature for the modelling of the SE-SR process, due to its low computational cost. In the E-E approach, both phases are described as interpenetrating continua, with individual conservation equations written and solved for the fluid and/or solid phases. The resulting averaged equation produces a set of unknowns that are solved using closure laws such as the constant particle viscosity (CPV), particle and gas turbulence (PGT), particle and gas turbulence with drift velocity (PGTDV), particle turbulence (PT) and kinetic theory of granular flows (KTGF). Majorly, the concept of kinetic theory of dense gases is applied to the granular solid flows to estimate the necessary constitutive correlations for the solid interfaces such as interphase momentum transfer, internal heat and mass transfer, solid pressure, stress tensors (see

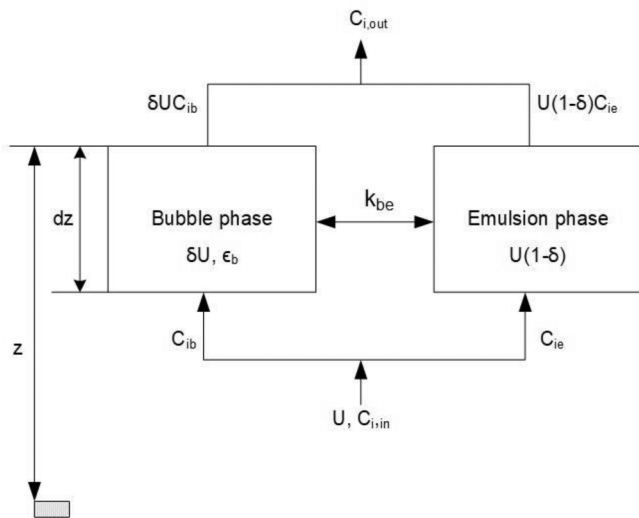


Fig. 7. Schematic of the differential slice for a two-phase fluidisation model.

Table 5
Governing equations for a CFD model in the Eulerian framework and some constitutive correlations and drag models.

Principles	Equations	Equation	Ref.
Continuity	$\frac{\partial}{\partial t}(\epsilon_k \rho_k) + \frac{\partial}{\partial x_i}(\epsilon_k \rho_k u_k) = S_{con}$	33	[103]
Momentum	$\left[\frac{\partial}{\partial t}(\epsilon_k \rho_k u_k) + \frac{\partial}{\partial x_j}(\epsilon_k \rho_k u_k u_{kj}) \right] = -\epsilon_k \frac{\partial P_k}{\partial x_j} + \frac{\partial \tau_{kij}}{\partial x_j} + \epsilon_k \rho_k g_i - M + S_{mom} u_k$	34	[103,104]
Species composition	$\frac{\partial}{\partial t}(\epsilon_k \rho_k X_{kn}) + \frac{\partial}{\partial x_i}(\epsilon_k \rho_k X_{kn} u_{ki}) = \frac{\partial}{\partial x_i} \left(D_{kn} \frac{\partial X_{kn}}{\partial x_i} \right) + S_{sp}$	35	[103]
Energy conservation	$\frac{\partial}{\partial t}(\epsilon_k \rho_k H_k) + \nabla \cdot (\epsilon_k \rho_k u_k H_k) = \nabla \cdot (\lambda_k \nabla T_k) + \Delta H_k + S_{en}$	36	[103]
Granular temperature	$\frac{3}{2} \epsilon_m \rho_m \left[\frac{\partial \Theta_m}{\partial t} + u_{mj} \frac{\partial \Theta_m}{\partial x_j} \right] = \frac{\partial}{\partial x_j} \left(\kappa_m \frac{\partial \Theta_m}{\partial x_j} \right) + \tau_{mij} \frac{\partial U_m}{\partial x_j} + \Pi_m - \gamma$	37	[103]
Solid pressure	$P_s = \epsilon_s \rho_s \Theta_s + 2 \epsilon_s^2 \rho_s \Theta_s g_{0,ss} (1 + e_{ss})$	38	[105]
Interfacial momentum force	$M = \beta (u_s - u_k)$	39	
Wen and Yu drag model	$\beta = \frac{3}{4} C_d \frac{\epsilon_p \epsilon_g \rho_g v_p - v_g }{d_p} \epsilon_g^{-2.65};$ $C_d = \frac{24}{\epsilon_g Re_p} \left[1 + 0.15 (\epsilon_g Re_p)^{0.687} \right]$	40	[106]
Gidaspow drag model	$\beta = 150 \frac{\epsilon_p (1 - \epsilon_g) \mu_g}{\epsilon_g d_p^2} + 1.75 \frac{\rho_g v_p - v_g }{d_p}, \epsilon_g \leq 0.80;$ $\beta = \frac{3}{4} C_d \frac{\epsilon_p \epsilon_g \rho_g u_p - u_g }{d_p} \epsilon_g^{-2.65}, \epsilon_g > 0.80;$ $C_d = \begin{cases} \frac{24}{\epsilon_g Re_p} \left[1 + 0.15 (\epsilon_g Re_p)^{0.687} \right], Re_p < 1000; \\ 0.44, Re_p \geq 1000 \end{cases}$	41	[107]
Syamlal-O'Brien drag model	$\beta = \frac{3 \epsilon_p \epsilon_g \rho_g}{4 v_{r,p}^2 d_p} C_d \left(\frac{Re_p}{v_{r,p}} \right) u_p - u_g ;$	42	[108]
Gibilaro drag model	$u_{r,p} = 0.5 \left(A - 0.06 Re_p + \sqrt{(0.06 Re_p)^2 + 0.12 Re_p (2B - A) + A^2} \right);$ $\beta = \left(\frac{17.3}{Re_p} + 0.336 \right) \frac{\rho_g u_g - u_s }{d_p} \epsilon_s \epsilon_g^{-1.8} Re_p = \frac{(1 - \epsilon_s) \rho_g u_g - u_s d_p}{\mu_g^m}$	43	[109]

Table 6
Summary of modelling activities for SE-SR in fluidised bed reactors.

References	Reactor concept	Operating conditions	Kinetic models			Modelling approach	Research outcome
Johnsen et al. [79]	<u>Dual BFB</u> D = -0.1 m	P = 1 bar; T = 873 K; S/C = 3-4; Gas velocity = 0.1 m/s	SMR Ref. [66]	Carbonation Ref. [79]	Calcination Ref. [79]	Steady-state two-phase model of Orcutt et al. [129]	<ul style="list-style-type: none"> To achieve > 90 % capture efficiency, reformer temperature between 540 °C and 630 °C is recommended.
Solsvik et al. [114,115,118]	<u>BFB, CFB</u> <u>Small</u> D = 0.1–0.2 m; H = 1 m <u>Large</u> D = 0.6 m; H = 4 m	T = 900 K; P = 1 and 10 bar; S/C = 3; Gas velocity = 0.2 m/s	Ref. [66]	Ref. [81]	–	CFD: 1-D Eulerian-Eulerian (two-fluid) model based on KTGF.	<ul style="list-style-type: none"> Model validation showed wide deviations when internal flow details were compared. Performance of SE-SR largely depends on reactor temperature.
Sanchez et al. [130]	<u>CFB</u> D = 1 m	T = 873 K; Gas velocity = 0.10 m/s; S/C = 4	Ref. [66]	Ref. [81]	Ref. [90]	CFD: 1-D Eulerian-Eulerian two-fluid model based on Constant Particle Viscosity (CPV); Gidaspow drag model	Low reformer temperature and high hydrogen yield was observed at low solid circulation rates.
Di Carlo et al. [117]	<u>BFB</u> ID = 0.25 m; H = 2 m; Bed height = 0.4 m	T = 923 K; P = 1 bar; gas velocity = 0.2–0.5 m/s; S/C ratio = 3	Ref. [65]	Ref. [80] and Ref. [82]	–	CFD: 2-D Eulerian-Eulerian two-fluid model based on KTGF; Gibilaro drag model.	<ul style="list-style-type: none"> At 100 % calcined sorbent condition, up to 95 % hydrogen purity can be obtained for all superficial velocities whereas at 50 % calcined sorbent, less than 85 % purity is obtainable.
Herce et al. [112,113]	<u>BFB</u> H = 1 and 4 m; D = 0.1 and 1 m	T = 600, 800 & 900 K; P = 1 & 7 bar; Superficial gas velocity = 0.1, 0.2 & 0.5 m/s; S/C ratio = 4	Ref. [66]	Ref. [80] and Ref. [81]	–	CFD: 2-D Eulerian-Eulerian two-fluid model based on KTGF; Syamlal-O'Brien drag model and Modified-Wang drag model	<ul style="list-style-type: none"> The effect of heat and mass transfer on SE-SR reaction is more apparent at large scale compared to the use of different sorbent. Carbonation reaction is the rate limiting step of SE-SMR process.
Phuakpunk et al. [111,131]	<u>CFB</u> <u>Riser</u> H = 7 m; ID = 0.05 and 0.2 m <u>Regenerator</u> D = 1.2 m; Bed height = 0.8 m	<u>Riser</u> T = 848 and 938 K; P = 1 bar; S/C = 4; Gas velocity = 4 and 6 m/s; <u>Regenerator</u> Gas velocity = 1 m/s	Ref. [66]	Ref. [81]	Ref. [90]	CFD: 2-D transient Eulerian-Eulerian two-fluid model based on KTGF; Gidaspow drag model	<ul style="list-style-type: none"> Hydrogen purity is influenced by design parameters other than reaction parameters, with gas velocity, the riser diameter and the solid flux having the most impact. Solid preheating to 950 °C is required to achieve CaO conversion of ~ 0 % when regenerator was scaled up to a double-stage bubbling bed.
Lindborg et al. [119]	<u>BFB</u> H = 0.687–5.496 m; D = 0.229–0.916 m	P = 10 bar; T = 848 K; Superficial velocity = 0.10 m/s; S/C = 5	Ref. [66]	Ref. [89]	–	CFD: 2-D Eulerian-Eulerian two-fluid model based on KTGF; Gibilaro drag model	<ul style="list-style-type: none"> Bed diameters have little effect on hydrogen production, therefore wide reactors are the best choice for high mass throughputs. Performance by heat supply through CFB exceeds the batch reactor wall heating.
Chen et al. [47,110]			Ref. [66]	Ref. [77] and Ref. [88]	–	CFD: 2-D transient Eulerian-Eulerian two-fluid model; three-fluid models based on	<ul style="list-style-type: none"> Under high velocities, large bubble sizes reduce CO₂ capture efficiency for the hydrotalcite sorbent, not necessarily gas residence time.

(continued on next page)

Table 6 (continued)

References	Reactor concept	Operating conditions	Kinetic models			Modelling approach	Research outcome
	<u>BFB</u> H = 1 m; D = 0.1 m	T = 773 K; P = 1 bar; Inlet velocity = 0.08–0.3 m/s				KTGF; Syamlal–O'Brien drag model and Gidaspow drag model	High content of CO and H ₂ in COG feed reduces methane conversion For the three-fluid approach, modelling SE-SR of COG with separate sorbent-catalyst system predicts product yield more accurately, compared with bifunctional catalysts system.
Di Carlo et al. [132]	<u>BFB</u> H = 0.6 m; ID = 10 cm; Bed height = 4 m	T = 900 K; Superficial gas velocity = 0.3 m/s; S/C ratio = 4	Ref. [66]	Ref. [79]	–	CFD: 2-D Eulerian-Eulerian three-fluid model based on KTGF; Gidaspow drag model and Syamlal-O'Brien drag model.	<ul style="list-style-type: none"> Considered intra and external mass transfer across the particles. With a dolomite/catalyst ratio greater than 2, a dry hydrogen mole fraction of more than 0.93 is predicted.
Wang et al. [126]	<u>BFB</u> H = 1.5 m; D = 0.3 m	T = 873 K; P = 1 bar; Gas velocity = 0.4–0.6 m/s	Ref. [69]	Ref. [87]	–	CFD: 3-D Eulerian-Eulerian multi-fluid model based on KTGF; EMMS drag model	<ul style="list-style-type: none"> Model considered the bubble impact on gas–solid drag force. Decreasing both sorbent diameter and operating velocity improve hydrogen yield and conversion.
Dat Vo et al. [133]	<u>CFB</u> <u>Reformer</u> H = 4 m D = 0.2 m <u>Regenerator</u> H = 3 m D = 0.2 m	<u>Reformer</u> T = 873–973 K; P = 1–10 bar; Gas velocity = 0.3 m/s S/C = 4.0–5.0 <u>Regenerator</u> T = [1163 + (P-1) * 15] K; P = 1–10 bar; Gas velocity = 2 m/s	Ref. [66]	Ref. [81]	Ref. [134]	CFD: 1-D dynamic Eulerian-Lagrange model.	<ul style="list-style-type: none"> Temperature has a significant impact on SE-SMR performance, cost and efficiency. In comparison to the SMR process, SESMR was found to achieve a high energy efficiency of 82.2 % and a 12 % decrease in the cost of producing blue H₂.
Wang et al. [127]	<u>BFB</u> H = 1.0 m; ID = 0.063 m	T = 673 K; P = 1 bar; Gas velocity = 1 m/s	Ref. [68]	Ref. [86]	–	CFD: 3D Eulerian-Lagrange (DDPM) model; Gidaspow drag model	<ul style="list-style-type: none"> Considering particle size distribution enhanced prediction of bed expansion height. High pressure favours CO₂ sorption over hydrogen production.
Yang et al. [135]	<u>ICFB</u> <u>Reformer</u> H = 0.7 m; D = 0.05 m; <u>Regenerator</u> H = 1.4 m; D = 0.05 m	T = 673 K; P = 1 bar; Gas velocity = 1 m/s <u>Regenerator</u> T = 673 K; P = 1 bar; Gas velocity = 2 m/s	Ref. [68]	Ref. [86]	Ref. [86]	CFD: 2D Eulerian-Lagrange (DDPM) model	<ul style="list-style-type: none"> Increasing the regenerator's velocity and solid loading promotes solids circulation but causes gas leakage.
Zhanghao et al. [128]	<u>BFB</u> H = 1 m; D = 0.1 m	T = 823 – 973 K; P = 1 bar; Gas velocity = 0.15 – 0.3 m/s	Ref. [66]	Ref. [80]	–	CFD: 3D Eulerian-Lagrange MP-PIC; Gidaspow drag model	<ul style="list-style-type: none"> Studied the interaction and behaviour of flow characteristics including bubble evolution and thermal parameters. Bed temperature and gas velocities influence product yields.

Table 5) [102]. Detailed description of these multiphase flow model equations and other corresponding parameters can be found in literature [103].

The conservation equations of mass, momentum and heat each contain the term $-S$, which can be a sink or source of these quantities. For instance, S in the mass conservation equation accounts for the mass transfer between the gas and solid phases due to the production and consumption of gas species from reforming and carbonation. The balanced rate of formation and consumption are derived for each of the gas components using the reforming and carbonation reaction rate expressions and inserted into their respective transport equations.

Conversely in the momentum equation, the pressure, viscous and interfacial forces are accounted for in the solid and gaseous phases. Additionally, to complete the momentum equation for the solid phase, a solid pressure, P_s , is included to the right-hand side of the equation. The interphase momentum force includes a drag function, β – an important parameter for describing hydrodynamics in fluidised bed reactors. This can be described by various drag models such as the Syamlal-O'Brien, Gidaspow, Energy minimization multi-scale (EMMS) and Gibilaro drag models; that have been applied to model SE-SR in fluidised bed reactors, as presented in Table 5. The energy conservation equation is written in terms of specific enthalpy, H and solved for phase k , where ΔH_k represents the heat of reaction. The mathematical models for SE-SR have been popularly solved using numerical techniques such as finite volume and finite difference methods in Ansys FLUENT, MFX and MATLAB respectively.

4. Status of modelling activities for SE-SR in fluidised bed reactors

This section highlights and analyses the state-of-the-art in modelling works applied to SE-SR and discusses the challenges and limitations associated with the models. Different models and modelling approaches have been employed to predict the performance of SE-SR in fluidised bed reactors. A summary of these modelling studies available in literature, including their kinetic model used and modelling approach, is presented in Table 6.

4.1. Two-phase models

One of the earliest models of SE-SR in fluidised bed reactors was developed using the conventional fluidisation model. Johnsen et al. [79] applied Orcutt's two-phase model to simulate SE-SR of methane in a bubbling fluidised bed reactor as described in section 3.2. The bubble phase was assumed to be without reaction and in plug flow regime, whereas the dense phase contains gases that are perfectly mixed. Their model applied the SMR kinetic model of Xu and Froment [66], the shrinking core model for carbonation/calcination and was implemented in MATLAB. Both reactors were solved in an iterative manner by guessing the initial temperature of solids input to the reformer until steady-state was achieved. Although this model is simple and was able to simulate SE-SR of methane, the assumption of stagnant solids, inability to account for flow details such as particle size distribution and internal circulation, and complex solution procedure restricts the use of this model, especially for scaleup studies.

Johnsen [98] also applied this conventional approach to model CFB riser for SE-SR of methane, based on the slip-factor criterion. He assumed a steady state plug flow for the catalyst, gas and sorbent in the reformer and determined the solid fraction, using the correlation proposed by Pugsley and Berruti [97]. Though the results obtained were not validated by any experiments, solid fraction was found to be the key parameter influencing the performance of SE-SR of methane, as seen in equation 44. Equation 44 represents the design equation for a riser model, assuming a constant solid fraction along the height of the reactor; where $1 - \epsilon$ is the solid fraction, F and r are the solid molar flow and the rate of reaction for species i , respectively. Increasing the solids flow rate

increases the solid fraction, which inadvertently leads to an increase in the reaction rate.

$$\frac{dF_i}{dz} = A_c(1 - \epsilon)r_i \quad (44)$$

The two-phase model has not been considered for a while in SE-SR process modelling. Moreover, technological advancement has accelerated the adoption of computer-based models such as CFD.

4.2. Two-fluid CFD models

Current modelling works for SE-SR in fluidised bed reactors, using a wide range of feedstocks and sorbents, are dominated by CFD models. In the two-fluid model, conservation equations are written and solved for two phases: one gas phase and one particulate phase (for both sorbent and catalyst) based on the Eulerian framework. This is different from the multi-fluid/three-fluid model where conservation equations are solved for all the phases involved in the process – one gaseous phase and two solid phases (catalyst and sorbent). However, in most cases, the sorbent and catalysts are assumed to have the same properties and constant size [110–117]. CFD simulation of SE-SR in fluidised bed reactors have been carried out based on different levels of model complexities; usually based on phase description and spatial dimensions (1D, 2D and 3D) of the computational domain. The phase description mentioned here depends on whether it is a two-fluid, three-fluid or E-L model.

A close inspection of literature reveals that majority of the modelling activities originate from a research group in the Norwegian University of Science and Technology, Norway. Their central research theme was on improving reactor models using codes developed inhouse. Transient behaviour studies have been led by Solsvik et al. [114,115,118], which was focused on developing a transient 1D two-fluid model and applying it to SE-SR process. The 1D two-fluid model was applied to the simulation of SE-SR of methane in a BFB reactor to investigate its performance compared with a 2D two-fluid model [118]. Granular temperature, which is the kinetic energy that describes the random velocities of the particles, was not considered in the model. The finite volume method was implemented to solve the model equation in MATLAB and FORTRAN programs. Model validation was performed using simulation results of species outlet composition obtained for a formulated 2D model. However, this 1D model was unable to accurately predict internal flow behaviours such as bed expansion and gas bypassing compared to the 2D model, and relatively small errors in the outlet CO₂ composition compared with experimental data were also observed. Fig. 8 shows the disparity in bed expansion between the 1D and 2D models. Larger bed expansion was predicted by the 1D model compared with the 2D model. The 1D model was also extended to the simulation of SE-SR of methane in a CFB reactor, where they discovered that reactor performance is largely impacted by the reactor temperature.

Compared to the one-dimensional model, a two-dimensional models can provide a more accurate prediction of gas–solid behaviours. Lindborg and Jakobsen [119] applied an axisymmetric 2D two-fluid model

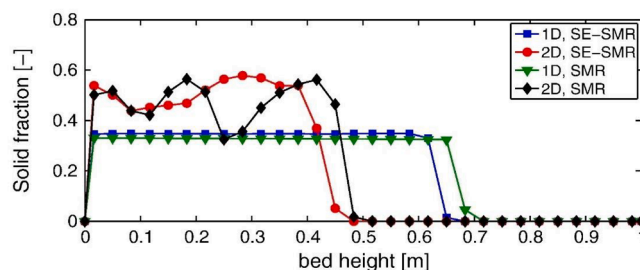


Fig. 8. Comparison of solid fractions in 1D and 2D modelling of SE-SR of methane in a BFB reactor (reused from Solsvik et al. [118], with permission from American Chemical Society).

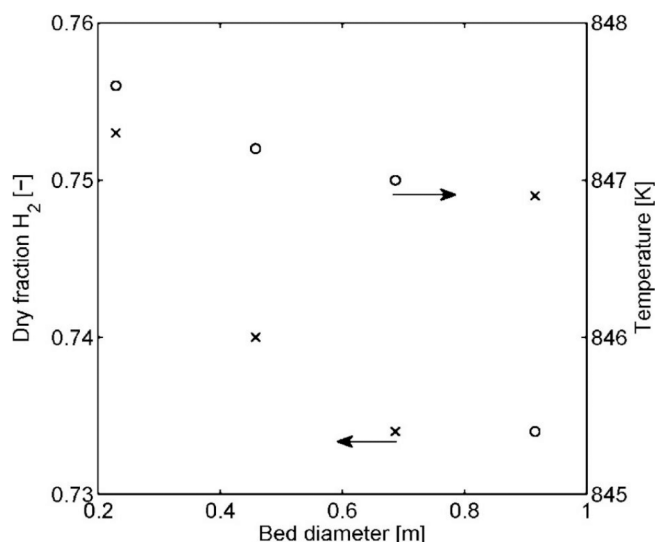


Fig. 9. Influence of bed diameter on outlet hydrogen concentration and temperature (reused from Lindborg and Jakobsen [119], with permission from American Chemical Society).

to investigate the performance of SE-SR in fluidised bed reactor under varying heat supply conditions and reactor widths. The kinetic models were incorporated via a user defined function (UDF) to a CFD software employing a finite volume method to solve the set of governing equations. In their work, an ozone decomposition reaction occurring in a BFB reactor was first modelled to compare simulation results of the gas–solid reaction with laboratory experiments (model validation), before applying the model to SE-SR of methane. Though slightly deviating results for the in-bed concentrations were obtained during model validation, the impact of different bed diameters on reactor performance was successfully demonstrated (see Fig. 9). Fig. 9 shows relatively low temperatures as bed diameter increases, whereas decreasing hydrogen concentration is observed up to a bed diameter of 0.91 m. However, this axisymmetric 2D may not sufficiently provide a very good prediction of reactor performance. This is because the resulting flow pattern can depict large concentration of catalyst-sorbent particles at the central axis, since particles are unable to pass through the axis, thus negatively impacting on the hydrogen output result.

In a study conducted by Hecce et al. [112], 2D two-fluid model based on KTGF, combined with the Taguchi method was used to perform a sensitivity analysis on variables including bed expansion, CO₂ concentration, methane conversion, hydrogen production, pressure drop and solid fraction for SE-SR of methane. The model predicted that hydrogen production is very sensitive to temperature. Also, increased gas–solid residence time, influenced to a great extent by hydrodynamics, was also observed to significantly affect hydrogen production. Carbonation reaction was also established to be the rate limiting step of SE-SR of methane, with hydrogen purity reaching 92 %.

Similarly, Phuakpunk et al. presented a simple 2D two-fluid model to simulate SE-SR of methane [111] and ethanol [120] in the riser of a CFB reactor. As with some other works, model validation was comparable for hydrogen output but showed great deviation for CO₂ concentration – about 40 %. The model was used in conjunction with a 2^k factorial design method to perform a sensitivity study and explore the relationship between process variables like catalyst-to-sorbent ratio, temperature and gas velocity, and the response variables: hydrogen flux and purity. While inlet temperature was reported to greatly affect hydrogen flux, overall hydrogen performance – hydrogen flux and purity – was shown to be significantly influenced by solid flux, gas velocity and riser diameter. Further, the response was optimised, and the hydrodynamics of the optimum case investigated. Their work represents the first attempt at optimising hydrogen production in a newly designed riser

reactor for SE-SR process. Although, their work did not present considerable information on sorbent performance, it has been established that only a part of sorbent's capacity is being utilised during SE-SR process in fluidised bed reactors [121]. Therefore, the use of riser may impact on equipment size and cost, as the problem of low residence time affecting sorbent utilisation in a riser is solved by increasing the riser height.

Conversely, a more elaborate 3D two-fluid model formulated by Wang et al. [122] and applied to the same process and particle properties disclosed the absence of this behaviour for the 3D simulation. The steady-state model also presented a more uniform temperature distribution across the bed, indicating complete mixing as shown in Fig. 10. In another work using the same model, they successfully investigated how hydrodynamic parameters such as the restitution coefficient and gas flow rates affect the reactions of SE-SR of methane [123]. It was pointed out that the effect of restitution coefficient was less significant compared with gas flow rate, as this variable is more apparent and dependent on the condition of the gas flow rates.

Nevertheless, the simplification of the catalyst-sorbent particle system neglects the internal transport phenomena occurring at the particulate level which could impact results of hydrogen evolution and carbon

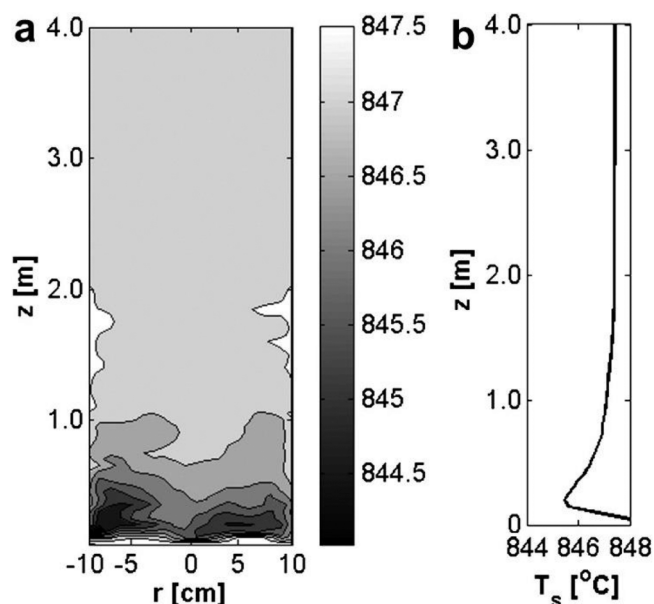


Fig. 10. Vertical cross-sectional (a) and axial (b) distributions of temperature in the reactor (reused from Wang et al. [122], with permission from Elsevier).

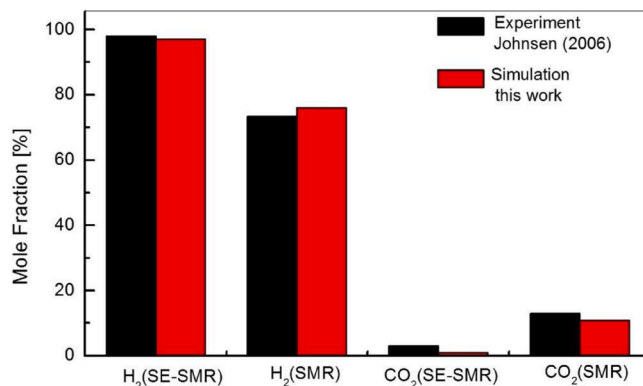


Fig. 11. Comparison of gas products (H₂ and CO₂) of SE-SMR and SMR obtained from experiment and 2D two-fluid model (reused from Chen et al. [110], with permission from Elsevier).

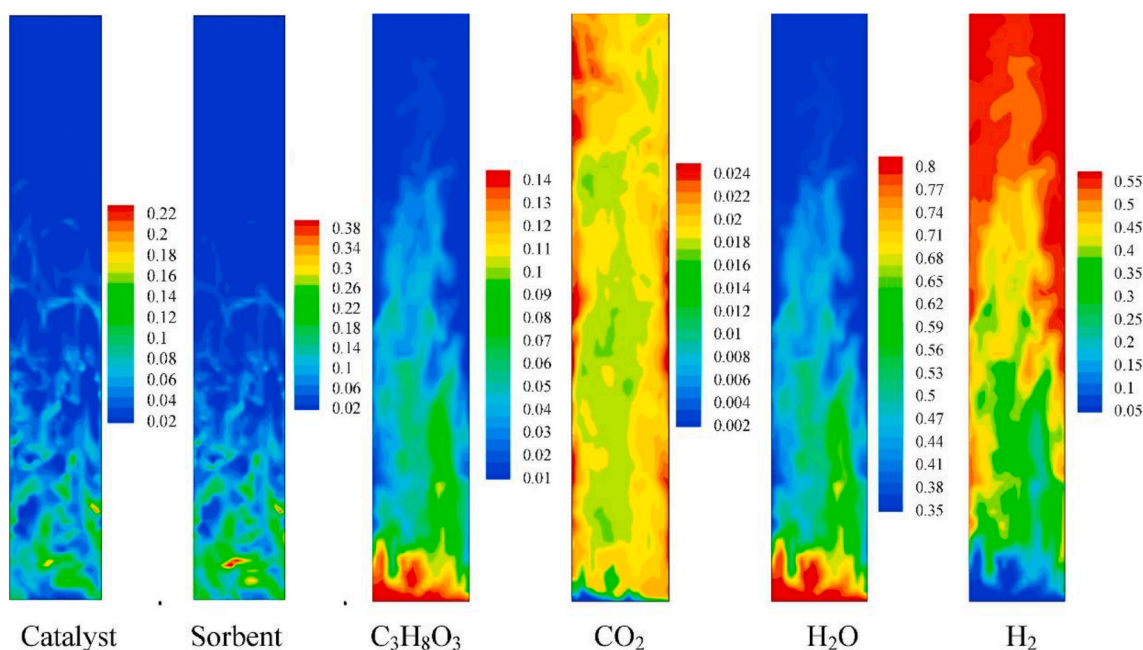


Fig. 12. Distribution of gas and solid concentrations (reused from Wang et al. [126], with permission from Elsevier).

capture. Moreover, Chen et al. [110] have revealed that assuming the same properties for both catalyst and sorbent particles generated a high error percent between simulation and experiments in the prediction of CO_2 concentration (see Fig. 11).

4.3. Three-fluid CFD models

Accordingly, a three-fluid approach, in which the catalyst and sorbent particles are considered as separate phases and a particle–particle drag term is introduced to couple both particles, is more suitable [20]. Such approach can enable the study of phenomena such as particle segregation—an indication of mixing behaviour—or separation, since for such two-pellet system, catalysts need to be separated from sorbent, for sorbent regeneration under high-temperature condition. With this approach, it is also possible to explore the impact of phenomena such as diffusion limitation on the particle scale, which is often neglected in SE-SR modelling. Though, in some steam reforming kinetic models, intra-particle and external diffusion limitation is usually accounted for using effectiveness factor, while that of carbonation is not often addressed. Chao et al. [125] presented a multifluid model for poly-disperse particles, introducing a semi-empirical frictional particle–particle drag term to account for the long term frictional contact of particles, combined with the collisional particle–particle drag. The model was able to demonstrate the segregation of catalyst and sorbent particles under varying operating conditions, as well as its impact on reactor performance for SE-SR of methane. The authors noted that segregation occurs at the start of the process due to the large density difference and heavier catalyst particles but becomes well-mixed as reaction proceeds due to sorbent conversion. Also, solids were reported to blend when the bed is run at 0.2 m/s, below which they segregate, with this velocity showing no direct impact on the purity of the hydrogen produced.

In an earlier study conducted by Di Carlo et al. [117], a this modelling approach was employed to investigate the hydrodynamics of SE-SR of methane in a lab-scale BFB reactor and compare results with the conventional SMR process. The 2D model considered intra and external mass transfer resistances in the development of the kinetic models for both catalyst and sorbent, and included a collisional

particle–particle drag which accounts for short term frictional contact of particles. However, model validation results appeared to underpredict bubble diameter and overestimate experiment data with a relatively large error (24 %) reported for CO_2 molar fraction in the output gas. The authors emphasised the need for a model to be further validated at a higher superficial velocity. The same multiscale reaction approach applied to the carbonation model was integrated by Chen et al. [47]. They formulated a 2D three-fluid model resembling Di Carlo et al.'s [117] to simulate SE-SR of coke oven gas in a BFB reactor. The model explored the two types of pellets designs applicable to SE-SR process: monofunctional pellets or two-pellet design where the sorbents and catalysts are modelled as separate particles, and bifunctional pellets or one-pellet design which integrate the sorbents and catalysts as a single particle. Modelling of sorbent pellets for SE-SR in fluidised beds was achieved by applying the shrinking unreacted core kinetic model which incorporates the three resistance terms – chemical reaction, intra-particle diffusion and external mass transfer in its rate equation. Meanwhile, for the bifunctional pellet, the external diffusion term is excluded since it is being accounted for by the effectiveness factor assigned to the catalysts. Simulation results were comparable to experimental results generated by the authors.

An upgraded 3D version of the three-fluid model has also been applied for the simulation of SE-SR process. In their work, Wang et al. [124,126] presented this 3D model to simulate SE-SR of biodiesel by-product and crude glycerol in BFB reactors. The model integrated a heterogeneous bubble-based drag model to resolve the mesoscale effect on the bubbling bed and was implemented in MFIX commercial program. Particle properties were assumed to have mean density and diameter and the multiscale approach for the chemical reactions was not considered. The result was also able to reveal the segregation behaviour between the highly dense sorbent particles and catalyst solids and the effect of their mixing behaviour on temperature distribution. In addition, they were able to study the behaviour of each of the solids (catalysts and sorbents) involved in the process, as well as the gas distribution, using contour plots. Fig. 12 shows the species and solids distribution in the reactor after 20 s simulation time.

4.4. Eulerian-Lagrange CFD models

E-L modelling approach solves for each individual particle using the Newton's second law of motion, easily accounting for particles of different size distribution and densities. Wang et al. [127] formulated a 3D DDPM model, which is an E-L hybrid model, in Fluent commercial code to study the performance of SE-SR of ethanol in a fluidised bed reactor. With the model, the particle size distribution was successfully used to analyse the bed expansion. Fig. 13 shows the difference in solids concentration and bed expansion when particle sizes distribution is considered. The influence of hydrogen distribution, outlet gas composition, temperature distribution, effect of catalyst to sorbent ratio and operating pressure on both CO₂ sorption and hydrogen production was

also studied.

DDPM model is limited to reactors with small number of particles or dilute particle flows, due to the computational power required for simulation. For larger loadings and process scale, the multiphase particle-in-cell (MP-PIC) model is more fitting and has recently been applied to simulate SE-SMR in a BFB reactor. In MP-PIC, particles are grouped as parcels, thus reducing the number of particles, and are modelled in the Lagrangian framework. Zhanghao et al. [128] adopted this model to simulate SE-SR of methane, where they analysed the impact of particle behaviours and bubble characteristics on the process performance. Fig. 14 shows the species distribution across the bubbles in the reactor. The concentrations of product gases are seen to increase along the bed height, with lower concentration observed for CO₂.

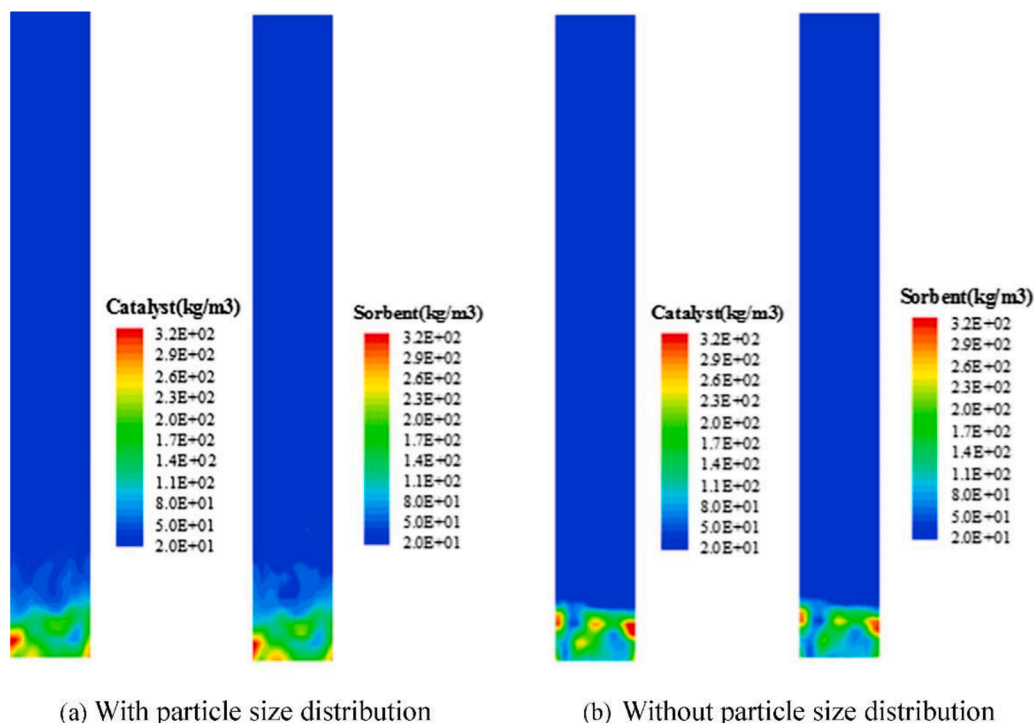


Fig. 13. Catalyst and sorbent distribution with and without particle size distribution (reused from Wang et al. [127], with permission from Elsevier).

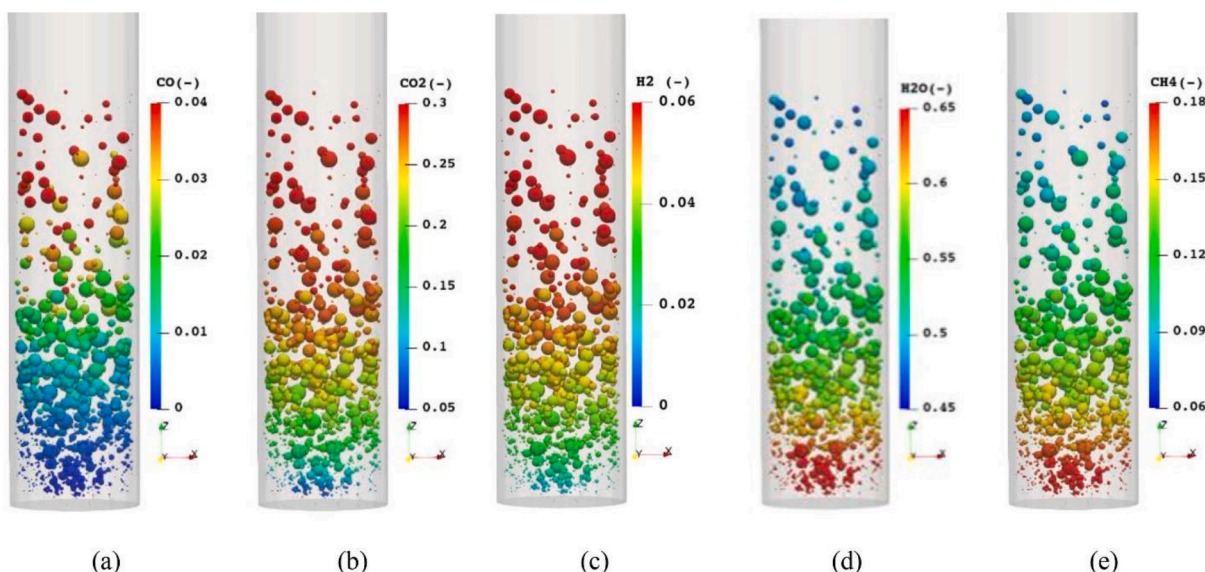


Fig. 14. Bubble distribution in the reactor described by gas species (reused from Zhanghao et al. [128], with permission from Elsevier).

4.5. Challenges and future perspectives

A major challenge in modelling the SE-SR process reactors remains the development of models that couple both reactor units in CFB configuration. CFB reactors allow for continuous circulation of sorbent particles between the reformer and regenerator, which is ideal for largescale SE-SR process. To date, no significant contribution has been made towards the extensive modelling and studying of a full-loop system (reforming/carbonation and calcination) for SE-SR, though this is usually attributed to the computational challenge of coupling both reactor units in the solution procedure.

For instance, Wang et al. [136] ran separate simulations of reforming/carbonation occurring in the downer (operating in bubbling flow regime) and regeneration in a riser using a 3D two-fluid model, without considering the solid flux between the reactors. Instead, the sorbent regenerator was investigated as a continuous operation where solids are allowed to leave and enter the boundaries at the outlet and inlet, respectively. Modelling the full-loop system is useful in studying the interactions between solid circulation rates and reaction parameters, since the conditions of the recycled solids from the calciner change. Influence of pressure drops across the reactors, entrainment, sorbent attrition and recovery can also be studied. Nonetheless, different strategies to achieve this coupling have been tried. One is a 3D Eulerian two-fluid model based on KTGF developed to model the carbonation/reforming of methane in a downer and sorbent regeneration in the riser of a CFB reactor by Wang et al. [137]. In their study, two sets of coordinates were used to simulate both reactors simultaneously in a CFD software using the same solid flux and time steps. Simulation results obtained at the outlets and inlets of both reactors are exchanged for each time step. Clearly, this simulation approach is prone to errors for a large simulation time due to its complexity. Alternatively, a simpler 1D two-fluid model applied to the simulation of SE-SR coupled in CFB reactors. Sanchez et al. [116] developed a 1D two-fluid model based on Constant Particle Viscosity closure to analyse SE-SR process in a CFB reactor. Both reactor units were coupled with the source terms for the solid phase species and energy conservation equations, and same pressure level was assumed for both units. This model was used to assess heat integration and solids flux under steady state conditions. However, the model was also reported to overestimate hydrogen yield and CO₂ sorption when compared with experimental data. Although simple, the use of the 1D model meant inability to study certain flow properties, as this model neglects performance along the radial direction.

There is also a challenge of 1D modelling for the transition zone between the dense bed and freeboard regions. Solsvik et al. [114] tried to resolve this in their dynamic 1D model of SE-SR in CFB reactors by introducing a tolerance condition for void fraction in the governing equation. Regardless, the model did not accurately predict bed expansion and other hydrodynamics and larger temperatures were recorded when compared with the base 2D model. Alternatively, Dat Vo et al. [133] applied the principle of coordinate transformation, where the bed height variable is converted to the different coordinate using the coordinate transformation equations. They simulated methane reforming/carbonation and regeneration in a CFB consisting of bubbling bed and fast fluidised bed reactors, respectively using a dynamic 1D Eulerian-Lagrangian two-phase model. Loss of flow details associated with this 1D model still makes it undesirable for purposes such as scaleup.

The low sorbent utilisation observed in fluidised bed reactors creates opportunities for studies into new reactor designs for SE-SR. Recently, a modelling study on a new reactor design coupling reforming/carbonation and regeneration processes was conducted by Yang et al. [135], who simulated SE-SR of ethanol in an internally circulating fluidised bed reactor using a 3D DDPM approach. Solid circulation was achieved by the transport of carbonated solids influenced by difference in pressure between both compartments, and the solids return from the regenerator section influenced by the descending velocity of the solids. However, it was found that while increased calciner velocity and solid loading

favours solid circulation, gas leakage between the reactors increases, thereby reducing hydrogen yield.

From previous paragraphs, it can be deduced that the different models and modelling approaches applied to SE-SR process can affect the prediction of process performance, although extensive modelling to compare these approaches is yet to be conducted. For one, drag models have been shown to affect the prediction of bed hydrodynamics. Chen et al. [110] applied two drag models – modified Syamlal-O'Brien and Gidaspow drag models – to simulate SE-SR of methane in a bubbling fluidised bed reactor and reported that the modified Syamlal-O'Brien overpredicted the bed expansion by 6 % whereas Gidaspow model gave a more accurate prediction at 2 % difference but overpredicted the minimum fluidisation velocity. Further validation of other drag models applied to the simulation of SE-SR process should be considered.

Some of the experiments used to validate the CFD models do not necessarily depict the conditions of the reactor being modelled. For instance, Shuai et al. [126] developed a CFD model for SE-SR of glycerol in a fluidised bed reactor and validated it with the experiment performed by Dou et al. [138] in a fixed bed reactor. Their model, although attributed to the negligence of catalyst deactivation in the model, overestimated the hydrogen volume fraction. Additionally, the percentage error between the simulated and experimental data for outlet methane composition was around 83 %. Therefore, more experimental works conducted in fluidised bed reactors are needed to enable validation of SE-SR reactor models.

Due to the high capital cost associated with carbon capture plants, it is more cost-effective to operate SE-SR at high pressure conditions, to reduce the energy penalty of compressing hydrogen downstream. This condition has recently been considered and modelled by few authors [139,140], but will still require validation with a much larger-scale test data. Modelling and validation of the process in fluidised bed reactors under such industrial conditions is crucial.

Solid materials involved in SE-SR in fluidised bed reactors will be subject to continuous multi-cycling, implying the need to consider decay and sintering of these materials, as well as loss in sorption activity over time. However, information on bifunctional materials under this condition is scarce in literature. It is necessary to develop correlations that represents the decline in sorbent activity during cycling, specific to these kinds of materials.

Finally, with the current advancement in computational capability and performance, opportunity lies in developing high-fidelity models for full-loop SE-SR process. This will allow further studies into the optimisation and improvement of heat transfer between both reactors, since previous studies have shown that this approach is better than directly heating the reformer.

5. Conclusion

Operating SE-SR technology in fluidised bed reactors is advantageous for the continuous production of high-purity blue hydrogen on a much larger scale. However, its TRL is low and developing a good model to predict largescale reactor performance can accelerate its scaleup and advancement. In this paper, the status of models and modelling activities applied to the study of SE-SR in fluidised bed reactors, is reviewed. Pilot tests and experimental activities in fluidised bed scenarios were also reviewed, since model validation is not complete without experiments.

CFD is the most adopted tool for modelling SE-SR in fluidised bed reactors, with models reportedly validated with lab scale experiments. More work remains to be done in modelling the full-loop SE-SR unit, comprising the reformer/carbonator and calciner. That way, it is possible to investigate and optimise heat transfer and thermal efficiency between both reactors, sorbent circulation rate required to improve CO₂ capture efficiency, and overall system performance. Investigation of SE-SR modelling in circulating fluidised bed reactors showed that low usage of sorbent sorption capacity is observed, hence, opportunity lies in the design and improvement of different configurations for the reformer/

carbonator and calciner. In addition, efforts are required in modelling and developing correlations for multifunctional catalyst pellets, as well as SE-SR model validation with real pilot scale data.

CRedit authorship contribution statement

Chinyelum Udemu: Conceptualization, Methodology, Visualization, Writing – original draft, Writing – review & editing. **Carolina Font-Palma:** Methodology, Supervision, Conceptualization, Writing – review & editing.

Declaration of Competing Interest

The authors declare that they have no known competing financial interests or personal relationships that could have appeared to influence the work reported in this paper.

Acknowledgment

The authors would like to acknowledge the funding provided by the Net Zero Research (formerly BF2RA) to undertake this research.

References

- [1] UNFCCC. Adoption of the Paris Agreement. 2015.
- [2] UNFCCC. The Race to Zero 2022. <https://climatechampions.unfccc.int/the-race-to-zero/> (accessed October 8, 2022).
- [3] Jeudy-Hugo S, Lo Re L, Falduto C. Understanding Countries' Net-Zero Emissions Targets. 2021.
- [4] Department for Business, Energy & Industrial Strategy (BEIS). Industrial Decarbonisation Strategy. 2021.
- [5] Abdin Z, Zafaranloo A, Rafiee A, Mérida W, Lipiński W, Khalilpour KR. Hydrogen as an energy vector. *Renew Sustain Energy Rev* 2020;120:109620. <https://doi.org/10.1016/j.rser.2019.109620>.
- [6] The Royal Society. Options for producing low-carbon hydrogen at scale. 2018.
- [7] Marbán G, Valdés-Solis T. Towards the hydrogen economy? *Int J Hydrogen Energy* 2007;32:1625–37. <https://doi.org/10.1016/j.ijhydene.2006.12.017>.
- [8] International Energy Agency (IEA). Net Zero by 2050 - A Roadmap for the Global Energy Sector. 2021.
- [9] British Petroleum (BP). Natural gas – Statistical Review of World Energy. 2021.
- [10] International Energy Agency (IEA). Hydrogen. Paris: 2021.
- [11] Navas-Anguila Z, García-Gusano D, Dufour J, Iribarren D. Revisiting the role of steam methane reforming with CO₂ capture and storage for long-term hydrogen production. *Sci Total Environ* 2021;771:145432. <https://doi.org/10.1016/j.scitotenv.2021.145432>.
- [12] Al-Qahtani A, Parkinson B, Hellgardt K, Shah N, Guillen-Gosalbez G. Uncovering the true cost of hydrogen production routes using life cycle monetisation. *Appl Energy* 2021;281:115958. <https://doi.org/10.1016/j.apenergy.2020.115958>.
- [13] Page B, Turan G, Zapantis A. Global Status of CCS 2020:2021.
- [14] Collidi G. Reference data and Supporting Literature Reviews for SMR Based Hydrogen Production with CCS. 2017.
- [15] Xu G, Jin H, Yang Y, Xu Y, Lin H, Duan L. A comprehensive techno-economic analysis method for power generation systems with CO₂ capture. *Int J Energy Res* 2010;34:321–32. <https://doi.org/10.1002/ER.1559>.
- [16] World Energy Council Netherlands. Hydrogen - Industry as Catalyst: Accelerating the Decarbonisation of our Economy to 2030. 2019.
- [17] Harrison DP. Sorption-enhanced hydrogen production: A review. *Industrial and Engineering Chemistry Research*, vol. 47, American Chemical Society; 2008, p. 6486–501. <https://doi.org/10.1021/ie800298z>.
- [18] Voldsund M, Jordal K, Anantharaman R. Hydrogen production with CO₂ capture. *Int J Hydrogen Energy* 2016;41:4969–92. <https://doi.org/10.1016/j.ijhydene.2016.01.009>.
- [19] Hanak DP, Michalski S, Manovic V. From post-combustion carbon capture to sorption-enhanced hydrogen production: A state-of-the-art review of carbonate looping process feasibility. *Energ Convers Manage* 2018;177:428–52. <https://doi.org/10.1016/j.enconman.2018.09.058>.
- [20] Wang J, Huang L, Yang R, Zhang Z, Wu J, Gao Y, et al. Recent advances in solid sorbents for CO₂ capture and new development trends. *Energy. Environ Sci* 2014; 7. <https://doi.org/10.1039/C4EE01647E>.
- [21] Di Giuliano A, Gallucci K. Sorption enhanced steam methane reforming based on nickel and calcium looping: a review. *Chem Eng Process - Process Intensif* 2018; 130:240–52. <https://doi.org/10.1016/j.cep.2018.06.021>.
- [22] Barelli L, Bidini G, Gallorini F, Servili S. Hydrogen production through sorption-enhanced steam methane reforming and membrane technology: A review. *Energy* 2008;33:554–70. <https://doi.org/10.1016/j.energy.2007.10.018>.
- [23] Wu Y-J, Li P, Yu J-G, Cunha AF, Rodrigues AE. Progress on sorption-enhanced reaction process for hydrogen production. *Rev Chem Eng* 2016. <https://doi.org/10.1515/revce-2015-0043>.
- [24] Romano MC, Martínez I, Murillo R, Arstad B, Blom R, Ozcan DC, et al. Process simulation of Ca-looping processes: review and guidelines. *Energy Procedia* 2013; 37:142–50. <https://doi.org/10.1016/j.egypro.2013.05.095>.
- [25] Masoudi Soltani S, Lahiri A, Bahzad H, Clough P, Gorbounov M, Yan Y. Sorption-enhanced Steam Methane Reforming for Combined CO₂ Capture and Hydrogen Production: A State-of-the-Art Review. *Carbon Capture Sci Technol* 2021;1: 100003. <https://doi.org/10.1016/J.CCST.2021.100003>.
- [26] Sikarwar VS, Pfeifer C, Ronsse F, Pohorelý M, Meers E, Kaviti AK, et al. Progress in in-situ CO₂-sorption for enhanced hydrogen production. *Prog Energy Combust Sci* 2022;91:101008. <https://doi.org/10.1016/J.PECS.2022.101008>.
- [27] Wilhelm G, Keller K, Schonfelder R, Klemp W. Production of hydrogen. *US1816523A*; 1931.
- [28] Hufton JR, Mayorga S, Sircar S. Sorption-enhanced reaction process for hydrogen production. *AIChE J* 1999;45:248–56. <https://doi.org/10.1002/aic.690450205>.
- [29] Berger AH, Bhowan AS. Optimizing solid sorbents for CO₂ capture. *Energy Procedia*, vol. 37, Elsevier Ltd; 2013, p. 25–32. <https://doi.org/10.1016/j.egypro.2013.05.081>.
- [30] Cherbański R, Molga E. Sorption-enhanced steam-methane reforming with simultaneous sequestration of CO₂ on fly ashes – Proof of concept and simulations for gas-solid-solid trickle flow reactor. *Chem Eng Process* 2018;124: 37–49. <https://doi.org/10.1016/j.cep.2017.11.010>.
- [31] Obradović A, Levec J. High purity hydrogen with sorption-enhanced steam methane reforming in a gas-solid trickle bed reactor. *Ind Eng Chem Res* 2017;56: 13301–9. <https://doi.org/10.1021/acs.iecr.7b01832>.
- [32] Kwang BY, Harrison DP. Low-pressure sorption-enhanced hydrogen production. *Ind Eng Chem Res* 2005;44:1665–9. <https://doi.org/10.1021/ie048883g>.
- [33] Ortiz AL, Balasubramanian B, Harrison DP. Combining steam-methane reforming, water-gas shift, and CO₂ removal in a single-step process for hydrogen production. Final report for period March 15, 1997 - December 14, 2000. Argonne, IL (United States): 2001. <https://doi.org/10.2172/807748>.
- [34] García-Lario AL, Grasa GS, Murillo R. Performance of a combined CaO-based sorbent and catalyst on H₂ production, via sorption enhanced methane steam reforming. *Chem Eng J* 2015;264:697–705. <https://doi.org/10.1016/j.cej.2014.11.116>.
- [35] Xie M, Zhou Z, Qi Y, Cheng Z, Yuan W. Sorption-enhanced steam methane reforming by in situ CO₂ capture on a CaO-Ca 9Al₆O₁₈ sorbent. *Chem Eng J* 2012;207–208:142–50. <https://doi.org/10.1016/j.cej.2012.06.032>.
- [36] Huang W-J, Yu C-T, Sheu W-J, Chen Y-C. The effect of non-uniform temperature on the sorption-enhanced steam methane reforming in a tubular fixed-bed reactor. *Int J Hydrogen Energy* 2021;46:16522–33. <https://doi.org/10.1016/j.ijhydene.2020.07.182>.
- [37] Neni A, Benguerba Y, Balsamo M, Erto A, Ernst B, Benachour D. Numerical study of sorption-enhanced methane steam reforming over Ni/Al₂O₃ catalyst in a fixed-bed reactor. *Int J Heat Mass Transf* 2021;165:120635. <https://doi.org/10.1016/j.ijheatmasstransfer.2020.120635>.
- [38] Chanburanasiri N, Ribeiro AM, Rodrigues AE, Arpornwichanop A, Laosiripojana N, Praserttham P, et al. Hydrogen production via sorption enhanced steam methane reforming process using Ni/CaO multifunctional catalyst. *Ind Eng Chem Res* 2011;50:13662–71. <https://doi.org/10.1021/ie201226j>.
- [39] Kim JN, Ko CH, Yi KB. Sorption enhanced hydrogen production using one-body CaO-Ca 12Al₁₄O₃₃-Ni composite as catalytic absorbent. *International Journal of Hydrogen Energy*, vol. 38, Pergamon; 2013, p. 6072–8. <https://doi.org/10.1016/j.ijhydene.2012.12.022>.
- [40] Aloisi I, Di Giuliano A, Di Carlo A, Foscolo PU, Courson C, Gallucci K. Sorption enhanced catalytic Steam Methane Reforming: Experimental data and simulations describing the behaviour of bi-functional particles. *Chem Eng J* 2017; 314:570–82. <https://doi.org/10.1016/j.cej.2016.12.014>.
- [41] Martavaltzi CS, Pampaka EP, Korkakaki ES, Lemonidou AA. Hydrogen production via steam reforming of methane with simultaneous CO₂ capture over CaO-Ca12Al14O33. *Energy and Fuels*, vol. 24, American Chemical Society; 2010, p. 2589–95. <https://doi.org/10.1021/ef9014058>.
- [42] Di Giuliano A, Giancaterino F, Courson C, Foscolo PU, Gallucci K. Development of a Ni-CaO-mayenite combined sorbent-catalyst material for multicycle sorption enhanced steam methane reforming. *Fuel* 2018;234:687–99. <https://doi.org/10.1016/j.fuel.2018.07.071>.
- [43] Chen H, Zhang T, Dou B, Dupont V, Williams P, Ghadiri M, et al. Thermodynamic analyses of adsorption-enhanced steam reforming of glycerol for hydrogen production. *Int J Hydrogen Energy* 2009;34:7208–22. <https://doi.org/10.1016/j.ijhydene.2009.06.070>.
- [44] Di Felice L, Kazi SS, Sorby MH, Martínez I, Grasa G, Maury D, et al. Combined sorbent and catalyst material for sorption enhanced reforming of methane under cyclic regeneration in presence of H₂O and CO₂. *Fuel Process Technol* 2019;183: 35–47. <https://doi.org/10.1016/j.fuproc.2018.10.012>.
- [45] Rackley SA. Adsorption capture systems. *Carbon Capture and Storage*, Elsevier; 2017, p. 151–85. <https://doi.org/10.1016/b978-0-12-812041-5.00007-6>.
- [46] Wu X, Wu S. Production of high-purity hydrogen by sorption-enhanced steam reforming process of methanol. *J Energy Chem* 2015;24:315–21. [https://doi.org/10.1016/S2095-4956\(15\)60317-5](https://doi.org/10.1016/S2095-4956(15)60317-5).
- [47] Chen Y, Grace JR, Zhao Y, Zhang J. Multi-fluid reactive modeling of sorption enhanced steam reforming of coke oven gas in fluidized bed. *Fuel* 2017;204: 152–70. <https://doi.org/10.1016/j.fuel.2017.05.031>.
- [48] Glier JC, Rubin ES. *Energy Procedia* 00 (2013) 000-000 Assessment of solid sorbents as a competitive post-combustion CO₂ capture technology Selection and/or peer-review under responsibility of GHGT. 2013.

- [49] Meloni E, Martino M, Palma V. A short review on Ni based catalysts and related engineering issues for methane steam reforming. *Catalysts* 2020;10:352. <https://doi.org/10.3390/catal10030352>.
- [50] Zhao C, Zhou Z, Cheng Z, Fang X. Sol-gel-derived, CaZrO₃-stabilized Ni/CaO-CaZrO₃ bifunctional catalyst for sorption-enhanced steam methane reforming. *Appl Catal B* 2016;196:16–26. <https://doi.org/10.1016/j.apcatb.2016.05.021>.
- [51] Balasubramanian B, Ortiz AL, Kaytakoglu S, Harrison DP. Hydrogen from methane in a single-step process. *Chem Eng Sci* 1999;54:3543–52. [https://doi.org/10.1016/S0009-2509\(98\)00425-4](https://doi.org/10.1016/S0009-2509(98)00425-4).
- [52] Abbas SZ, Dupont V, Mahmud T. Modelling of H₂ production in a packed bed reactor via sorption enhanced steam methane reforming process. *Int J Hydrogen Energy* 2017;42:18910–21.
- [53] Johnsen K, Ryu HJ, Grace JR, Lim CJ. Sorption-enhanced steam reforming of methane in a fluidized bed reactor with dolomite as CO₂-acceptor. *Chem Eng Sci* 2006;61:1195–202. <https://doi.org/10.1016/j.ces.2005.08.022>.
- [54] Hildebrand N, Readman J, Dahl IM, Blom R. Sorbent enhanced steam reforming (SESR) of methane using dolomite as internal carbon dioxide absorbent: Limitations due to Ca(OH)₂ formation. *Appl Catal A* 2006;303:131–7. <https://doi.org/10.1016/j.apcata.2006.02.015>.
- [55] Martínez I, Grasa G, Meyer J, Di Felice L, Kazi S, Sanz C, et al. Performance and operating limits of a sorbent-catalyst system for sorption-enhanced reforming (SER) in a fluidized bed reactor. *Chem Eng Sci* 2019;205:94–105. <https://doi.org/10.1016/j.ces.2019.04.029>.
- [56] García R, Gil MV, Rubiera F, Chen D, Pevida C. Renewable hydrogen production from biogas by sorption enhanced steam reforming (SESR): A parametric study. *Energy* 2021;218:119491. <https://doi.org/10.1016/j.energy.2020.119491>.
- [57] Cranfield University, Gas Technology Institute, The Babcock Doosan. Bulk Hydrogen Production by Sorbent Enhanced Steam Reforming (HyPER) Project. 2019.
- [58] IFE Hynor Hydrogen Technology Center (IFE Hynor) - IFE n.d. <https://ife.no/en/laboratory/ife-hynor-hydrogen-technology-center-ife-hynor/> (accessed September 25, 2021).
- [59] Meyer J, Mastin J, Bjørnebole TK, Ryberg T, Eldrup N. Techno-economical study of the Zero Emission Gas power concept. *Energy Procedia* 2011;4:1949–56. <https://doi.org/10.1016/j.egypro.2011.02.075>.
- [60] Mays J. One step hydrogen generation through sorption enhanced reforming. Golden, CO (United States): 2017. <https://doi.org/10.2172/1373949>.
- [61] Mays J, Stanis R. Techno-economic analysis for GTT's compact hydrogen generator. United States: 2020.
- [62] Lesemann M. Hydrogen production with integrated CO₂ capture. 2019.
- [63] Akers WW, Camp DP. Kinetics of the methane-steam reaction. *AIChE J* 1955;1:471–5. <https://doi.org/10.1002/aic.690010415>.
- [64] Allen DW, Gerhard ER, Likins MR. Kinetics of the methane-steam reaction. *Ind Eng Chem Process Des Dev* 1975;14:256–9. <https://doi.org/10.1021/i260055a010>.
- [65] Numaguchi T, Kikuchi K. Intrinsic kinetics and design simulation in a complex reaction network; steam-methane reforming. Tenth International Symposium on Chemical Reaction Engineering 1988:2295–301. <https://doi.org/10.1016/B978-0-08-036969-3.50086-5>.
- [66] Xu J, Froment GF. Methane steam reforming, methanation and water-gas shift: I. Intrinsic kinetics. *AIChE J* 1989;35:88–96. <https://doi.org/10.1002/aic.690350109>.
- [67] Zepieri M, Villa PL, Verdone N, Scarsella M, De Filippis P. Kinetic of methane steam reforming reaction over nickel- and rhodium-based catalysts. *Appl Catal A* 2010;387:147–54. <https://doi.org/10.1016/j.apcata.2010.08.017>.
- [68] Wu YJ, Santos JC, Li P, Yu JG, Cunha AF, Rodrigues AE. Simplified kinetic model for steam reforming of ethanol on a Ni/Al₂O₃ catalyst. *Can J Chem Eng* 2014;92:116–30. <https://doi.org/10.1002/CJCE.21773>.
- [69] Cheng CK, Foo SY, Adesina AA. Glycerol steam reforming over bimetallic Co-Ni/Al₂O₃. *Ind Eng Chem Res* 2010;49:10804–17. https://doi.org/10.1021/IE100462T/ASSET/IMAGES/IE-2010-00462T_M067.GIF.
- [70] Soliman MA, Adris AM, Al-Ubaid AS, El-Nashaie SSEH. Intrinsic kinetics of nickel/calcium aluminate catalyst for methane steam reforming. *J Chem Technol Biotechnol* 1992;55:131–8. <https://doi.org/10.1002/jctb.280550206>.
- [71] Katheria S, Kunzru D, Deo G. Kinetics of steam reforming of methane on Rh-Ni/MgAl₂O₄ catalyst. *React Kinet Mech Catal* 2020;130:91–101. <https://doi.org/10.1007/s11144-020-01767-y>.
- [72] Sugihara S, Kawamura Y, Iwai H. Rate equation of steam-methane reforming reaction on Ni-YSZ cermet considering its porous microstructure. *Journal of Physics: Conference Series*, vol. 745, Institute of Physics Publishing; 2016, p. 032147. <https://doi.org/10.1088/1742-6596/745/3/032147>.
- [73] Hou K, Hughes R. The kinetics of methane steam reforming over a Ni-/Al₂O₃ catalyst. vol. 82. 2001.
- [74] Mosayebi A, Nasabi M. Steam methane reforming on LaNiO₃ perovskite-type oxide for syngas production, activity tests, and kinetic modeling. *Int J Energy Res* 2020;44:5500–15. <https://doi.org/10.1002/er.5300>.
- [75] Mas V, Bergamini ML, Baronetti G, Amadeo N, Laborde M. A kinetic study of ethanol steam reforming using a nickel based catalyst. *Top Catal* 2008;51:39–48. <https://doi.org/10.1007/S11244-008-9123-Y/TABLES/4>.
- [76] Wang Y, Memon MZ, Seelro MA, Fu W, Gao Y, Dong Y, et al. A review of CO₂ sorbents for promoting hydrogen production in the sorption-enhanced steam reforming process. *Int J Hydrogen Energy* 2021. <https://doi.org/10.1016/j.ijhydene.2021.01.206>.
- [77] Rusten HK, Ochoa-Fernández E, Lindborg H, Chen D, Jakobsen HA. Hydrogen production by sorption-enhanced steam methane reforming using lithium oxides as CO₂-acceptor. *Ind Eng Chem Res* 2007;46:8729–37. <https://doi.org/10.1021/ie070770k>.
- [78] Pedunlik-Hofman L, Bayon A, Donne SW. Kinetics of solid-gas reactions and their application to carbonate looping systems. *Energies* 2019;12. <https://doi.org/10.3390/en12152981>.
- [79] Johnsen K, Grace JR, Elnashaie SSEH, Kolbeinsen L, Eriksen D. Modeling of sorption-enhanced steam reforming in a dual fluidized bubbling bed reactor. *Ind Eng Chem Res* 2006;45:4133–44. <https://doi.org/10.1021/ie0511736>.
- [80] Stendardo S, Foscolo PU. Carbon dioxide capture with dolomite: A model for gas-solid reaction within the grains of a particulate sorbent. *Chem Eng Sci* 2009;64:2343–52. <https://doi.org/10.1016/j.ces.2009.02.009>.
- [81] Sun P, Grace JR, Lim CJ, Anthony EJ. Determination of intrinsic rate constants of the CaO-CO₂ reaction. *Chem Eng Sci* 2008;63:47–56. <https://doi.org/10.1016/j.ces.2007.08.055>.
- [82] Aloisi I, Jand N, Stendardo S, Foscolo PU. Hydrogen by sorption enhanced methane reforming: A grain model to study the behavior of bi-functional sorbent-catalyst particles. *Chem Eng Sci* 2016;149:22–34. <https://doi.org/10.1016/j.ces.2016.03.042>.
- [83] Bhatia SK, Perlmutter DD. A random pore model for fluid-solid reactions: I. Isothermal, kinetic control. *AIChE J* 1980;26. <https://doi.org/10.1002/aic.690260308>.
- [84] Li ZS, Cai NS. Modeling of multiple cycles for sorption-enhanced steam methane reforming and sorbent regeneration in fixed bed reactor. *Energy Fuel* 2007;21:2909–18. <https://doi.org/10.1021/ef070112c>.
- [85] Lee D. An apparent kinetic model for the carbonation of calcium oxide by carbon dioxide. *Chem Eng J* 2004;100:71–7. <https://doi.org/10.1016/j.ces.2003.12.003>.
- [86] Ding Y, Alpay E. Equilibria and kinetics of CO₂ adsorption on hydroxylated adsorbent. *Chem Eng Sci* 2000;55:3461–74. [https://doi.org/10.1016/S0009-2509\(99\)00596-5](https://doi.org/10.1016/S0009-2509(99)00596-5).
- [87] Iliuta I, Radfarnia HR, Iliuta MC. Hydrogen production by sorption-enhanced steam glycerol reforming: sorption kinetics and reactor simulation 2012. <https://doi.org/10.1002/aic.13979>.
- [88] Reijers HTJ, Boon J, Elzinga GD, Cobden PD, Haije WG, Van Den Brink RW. Modeling study of the sorption-enhanced reaction process for CO₂ capture. I. Model development and validation. *Ind Eng Chem Res* 2009;48:6966–74. <https://doi.org/10.1021/ie801319q>.
- [89] Ochoa-Fernández E, Rusten HK, Jakobsen HA, Rønning M, Holmen A, Chen D. Sorption enhanced hydrogen production by steam methane reforming using Li₂ZrO₃ as sorbent: Sorption kinetics and reactor simulation. *Catal Today* 2005;106:41–6. <https://doi.org/10.1016/j.cattod.2005.07.146>.
- [90] Okunev AG, Nesterenko SS, Lysikov AI. Decarbonation rates of cycled CaO adsorbents. *Energy Fuel* 2008;22:1911–6. <https://doi.org/10.1021/ef800047b>.
- [91] Johnstone HF, Toomey RD. Gas fluidization of solid particles. *Chem Eng Prog* 1952;48:220.
- [92] Kunii D, Levenspiel O, Brenner H. *Fluidization engineering*. 2nd ed. Elsevier Science; 1991.
- [93] Davidson JF, Harrison D. *Fluidised particles*. Cambridge University Press; 1963.
- [94] Lee A, Miller DC. A one-dimensional (1-D) three-region model for a bubbling fluidized-bed adsorber. 121219160808001 *Ind Eng Chem Res* 2012;52. <https://doi.org/10.1021/ie300840q>.
- [95] Wen CY, Yu YH. A generalized method for predicting the minimum fluidization velocity. *AIChE J* 1966;12:610–2. <https://doi.org/10.1002/aic.690120343>.
- [96] Mori S, Wen CY. Estimation of bubble diameter in gaseous fluidized beds. *AIChE J* 1975;21:109–15. <https://doi.org/10.1002/aic.690210114>.
- [97] Pugsley TS, Berruti F. A predictive hydrodynamic model for circulating fluidized bed risers. *Power Technol* 1996;89:57–69. [https://doi.org/10.1016/S0032-5910\(96\)03154-3](https://doi.org/10.1016/S0032-5910(96)03154-3).
- [98] Johnsen K. *Sorption-enhanced steam methane reforming in fluidized bed reactors*. NTNU-trykk; 2006.
- [99] Gidaspow D. Hydrodynamics of fluidization and heat transfer: Supercomputer modeling. *Appl Mech Rev* 1986;39:1–23. <https://doi.org/10.1115/1.3143702>.
- [100] Lettieri P, Mazzei L. Challenges and issues on the CFD modeling of fluidized beds: A review. *J Comput Multiphase Flows* 2009;1:83–131. <https://doi.org/10.1260/175748209789563937>.
- [101] Jain V, Kalo L, Kumar D, Pant HJ, Upadhyay RK. Experimental and numerical investigation of liquid-solid binary fluidized beds: Radioactive particle tracking technique and dense discrete phase model simulations. *Particuology* 2017;33:112–22. <https://doi.org/10.1016/j.partic.2016.07.011>.
- [102] Hå L, Lysberg M, Jakobsen HA. Practical validation of the two-fluid model applied to dense gas-solid flows in fluidized beds. *Chem Eng Sci* 2007;62:5854–69. <https://doi.org/10.1016/j.ces.2007.06.011>.
- [103] Jakobsen HA. *Chemical reactor modeling: Multiphase reactive flows: Second edition*. vol. 9783319050928. Springer International Publishing; 2014. <https://doi.org/10.1007/978-3-319-05092-8>.
- [104] Adnan M, Sun J, Ahmad N, Wei JJ. Comparative CFD modeling of a bubbling bed using a Eulerian-Eulerian two-fluid model (TFM) and a Eulerian-Lagrangian dense discrete phase model (DDPM). *Powder Technol* 2021;383:418–42. <https://doi.org/10.1016/j.powtec.2021.01.063>.
- [105] Lun CKK, Savage SB, Jeffrey DJ, Chepurmy N. Kinetic theories for granular flow: inelastic particles in Couette flow and slightly inelastic particles in a general flowfield. *J Fluid Mech* 1984;140:223–56. <https://doi.org/10.1017/S0022112084000586>.
- [106] Wen CY, Yu YH. *Mechanics of fluidization*. *Chem Eng Prog Symp Ser* 1966;62:100–11.
- [107] Gidaspow D. *Multiphase flow and fluidization : continuum and kinetic theory descriptions* 1994:467.

- [108] Syamlal M, O'Brien TJ. Computer simulation of bubbles in a fluidized bed. *AIChE Symp. Ser.*, vol. 85, Publ by AIChE; 1989, p. 22–31.
- [109] Gibilaro LG, Di Felice R, Waldram SP, Foscolo PU. A predictive model for the equilibrium composition and inversion of binary-solid liquid fluidized beds. *Chem Eng Sci* 1986;41:379–87. [https://doi.org/10.1016/0009-2509\(86\)87017-8](https://doi.org/10.1016/0009-2509(86)87017-8).
- [110] Chen Y, Zhao Y, Zheng C, Zhang J. Numerical study of hydrogen production via sorption-enhanced steam methane reforming in a fluidized bed reactor at relatively low temperature. *Chem Eng Sci* 2013;92:67–80. <https://doi.org/10.1016/j.ces.2013.01.024>.
- [111] Phuakpunk K, Chalermainsuwan B, Putivisutisak S, Assabumrungrat S. Parametric study of hydrogen production via sorption enhanced steam methane reforming in a circulating fluidized bed riser. *Chem Eng Sci* 2018;192:1041–57. <https://doi.org/10.1016/j.ces.2018.08.042>.
- [112] Herce C, Cortés C, Stendardo S. Numerical simulation of a bubbling fluidized bed reactor for sorption-enhanced steam methane reforming under industrially relevant conditions: Effect of sorbent (dolomite and CaO-Ca12Al14O33) and operational parameters. *Fuel Process Technol* 2019;186:137–48. <https://doi.org/10.1016/j.fuproc.2019.01.003>.
- [113] Herce C, Cortés C, Stendardo S. Computationally efficient CFD model for scale-up of bubbling fluidized bed reactors applied to sorption-enhanced steam methane reforming. *Fuel Process Technol* 2017;167:747–61. <https://doi.org/10.1016/j.fuproc.2017.07.003>.
- [114] Solsvik J, Sánchez RA, Chao Z, Jakobsen HA. Simulations of steam methane reforming/sorption-enhanced steam methane reforming bubbling fluidized bed reactors by a dynamic one-dimensional two-fluid model: implementation issues and model validation. *Ind Eng Chem Res* 2013;52:4202–20. <https://doi.org/10.1021/ie303348r>.
- [115] Solsvik J, Chao Z, Jakobsen HA. Modeling and simulation of bubbling fluidized bed reactors using a dynamic one-dimensional two-fluid model: The sorption-enhanced steam-methane reforming process. *Adv Eng Softw* 2015;80:156–73. <https://doi.org/10.1016/j.advengsoft.2014.09.011>.
- [116] Sánchez RA, Chao Z, Solsvik J, Jakobsen HA. One dimensional two-fluid model simulations of the SE-SMR process operated in a circulating fluidized bed reactor. *Procedia Eng* 2012;42:1282–91. <https://doi.org/10.1016/J.PROENG.2012.07.520>.
- [117] Di Carlo A, Aloisi I, Jand N, Stendardo S, Foscolo PU. Sorption enhanced steam methane reforming on catalyst-sorbent bifunctional particles: A CFD fluidized bed reactor model. *Chem Eng Sci* 2017;173:428–42. <https://doi.org/10.1016/j.ces.2017.08.014>.
- [118] Solsvik J, Chao Z, Sánchez RA, Jakobsen HA. Numerical investigation of steam methane reforming with CO₂-capture in bubbling fluidized bed reactors. *Fuel Process Technol* 2014;125:290–300. <https://doi.org/10.1016/J.FUPROC.2014.03.039>.
- [119] Lindborg H, Jakobsen HA. Sorption enhanced steam methane reforming process performance and bubbling fluidized bed reactor design analysis by use of a two-fluid model. *Ind Eng Chem Res* 2009;48:1332–42. <https://doi.org/10.1021/ie800522p>.
- [120] Phuakpunk K, Chalermainsuwan B, Putivisutisak S, Assabumrungrat S. Factorial design analysis of parameters for the sorption-enhanced steam reforming of ethanol in a circulating fluidized bed riser using CFD. *RSC Adv* 2018;8:24209–30. <https://doi.org/10.1039/C8RA03901A>.
- [121] Arstad B, Blom R, Bakken E, Dahl I, Jakobsen JP, Røkke P. Sorption-enhanced methane steam reforming in a circulating fluidized bed reactor system. *Energy Procedia* 2009;1:715–20. <https://doi.org/10.1016/j.egypro.2009.01.094>.
- [122] Wang Y, Chao Z, Jakobsen HA. 3D Simulation of bubbling fluidized bed reactors for sorption enhanced steam methane reforming processes. *J Nat Gas Sci Eng* 2010;2:105–13. <https://doi.org/10.1016/j.jngse.2010.04.004>.
- [123] Wang Y, Chao Z, Jakobsen HA. Effects of gas-solid hydrodynamic behavior on the reactions of the sorption enhanced steam methane reforming process in bubbling fluidized bed reactors. *Ind Eng Chem Res* 2011;50:8430–7. <https://doi.org/10.1021/ie102330d>.
- [124] Wang S, Yang X, Xu S, Zhang K, Li B. Assessment of sorption-enhanced crude glycerol steam reforming process via CFD simulation. *Int J Hydrogen Energy* 2018;43:14996–5004. <https://doi.org/10.1016/J.IJHYDENE.2018.06.053>.
- [125] Chao Z, Zhang Y, Wang Y, Jakobsen JP, Jakobsen HA. Modelling of binary fluidized bed reactors for the sorption-enhanced steam methane reforming process. *Can J Chem Eng* 2017;95:157–69. <https://doi.org/10.1002/cjce.22602>.
- [126] Wang S, Yang X, Xu S, Zhang K, Li B. Evaluation of sorption-enhanced reforming of biodiesel-by-product in fluidized beds by means of CFD approach. *Fuel* 2018; 214:115–22. <https://doi.org/10.1016/J.FUEL.2017.10.128>.
- [127] Wang S, Xu S, Liu S, Hu B. Prediction of sorption-enhanced reforming process on hydrotalcite sorbent in a fluidized bed reactor. *Energy Conver Manage* 2019;180: 924–30.
- [128] Wan Z, Yang S, Bao G, Hu J, Wang H. Multiphase particle-in-cell simulation study of sorption enhanced steam methane reforming process in a bubbling fluidized bed reactor. *Chem Eng J* 2022;429:132461. <https://doi.org/10.1016/J.CEJ.2021.132461>.
- [129] Orcutt JC, Davidson JF, Pigford RL. Reaction time distributions in fluidized catalytic reactors. *Chem Eng Prog Symp Ser* 1962;58:1–15.
- [130] Sánchez RA, Chao Z, Solsvik J, Jakobsen HA. An investigation of the heat integration between the two riser units constituting a circulating fluidized bed reactor for the SE-SMR process. *Energy Procedia*, vol. 37, Elsevier Ltd; 2013, p. 1218–27. <https://doi.org/10.1016/j.egypro.2013.05.220>.
- [131] Phuakpunk K, Chalermainsuwan B, Putivisutisak S, Assabumrungrat S. Simulations of sorbent regeneration in a circulating fluidized bed system for sorption enhanced steam reforming with dolomite. *Particuology* 2020;50:156–72. <https://doi.org/10.1016/j.partic.2019.08.005>.
- [132] Di CA, Bocci E, Zuccari F, Dell'era A. Numerical investigation of sorption enhanced steam methane reforming process using computational fluid dynamics Eulerian-Eulerian code. *Ind Eng Chem Res* 2010;49:1561–76. <https://doi.org/10.1021/ie900748t>.
- [133] Dat Vo N, Kang JH, Oh M, Lee CH. Dynamic model and performance of an integrated sorption-enhanced steam methane reforming process with separators for the simultaneous blue H₂ production and CO₂ capture. *Chem Eng J* 2021;423: 130044. <https://doi.org/10.1016/J.CEJ.2021.130044>.
- [134] Martínez I, Grasa G, Murillo R, Arias B, Abanades JC. Kinetics of calcination of partially carbonated particles in a Ca-looping system for CO₂ capture. *Energy Fuel* 2012;26:1432–40. <https://doi.org/10.1021/ef201525k>.
- [135] Yang X, Wang S, Li B, Liu H, He Y. Evaluation of sorption-enhanced reforming over catalyst-sorbent bi-functional particles in an internally circulating fluidized bed. *Adv Powder Technol* 2020;31:2566–72. <https://doi.org/10.1016/j.apt.2020.04.020>.
- [136] Wang Y, Chao Z, Chen D, Jakobsen HA. SE-SMR process performance in CFB reactors: Simulation of the CO₂ adsorption/desorption processes with CaO based sorbents. *Int J Greenhouse Gas Control* 2011;5:489–97. <https://doi.org/10.1016/j.ijggc.2010.09.001>.
- [137] Wang J, Wang Y, Jakobsen HA. The modeling of circulating fluidized bed reactors for SE-SMR process and sorbent regeneration. *Chem Eng Sci* 2014;108:57–65. <https://doi.org/10.1016/j.ces.2013.12.012>.
- [138] Dou B, Dupont V, Rickett G, Blakeman N, Williams PT, Chen H, et al. Hydrogen production by sorption-enhanced steam reforming of glycerol. *Bioresour Technol* 2009;100:3540–7. <https://doi.org/10.1016/j.biortech.2009.02.036>.
- [139] Abbas SZ, Dupont V, Mahmud T. Kinetics study and modelling of steam methane reforming process over a NiO/Al₂O₃ catalyst in an adiabatic packed bed reactor. *Int J Hydrogen Energy* 2017;42:2889–903. <https://doi.org/10.1016/j.ijhydene.2016.11.093>.
- [140] Faheem HH, Tanveer HU, Abbas SZ, Maqbool F. Comparative study of conventional steam-methane-reforming (SMR) and auto-thermal-reforming (ATR) with their hybrid sorption enhanced (SE-SMR & SE-ATR) and environmentally benign process models for the hydrogen production. *Fuel* 2021;297:120769.